Structural relaxation of P_b defects at the (111)Si/SiO_2 interface as a function of oxidation temperature: The P_b-generation–stress relationship

A. Stesmans
Departement Natuurkunde, Universiteit Leuven, 3001 Leuven, Belgium
(Received 23 October 1992)

Electron-spin-resonance (ESR) studies of intrinsic P_b defects at the (111)Si/SiO_2 interface have been carried out as a function of oxidation temperature T_{ox} for the range $22 < T_{ox} < 1140$ °C. The properties of both as-oxidized structures and structures obtained after exhaustive dehydrogenation have been compared, thus separating the H passivation factor. The data reveal drastic differences in the interfacial nature of low-T_{ox} and high-T_{ox} Si/SiO_2 structures, the demarcation range being $\approx$750–850 °C; while a fairly constant density $(P_b) \sim 10^{13}$ cm^{-2} is found all over the range $300 < T_{ox} < 800$ °C, it gradually decreases with increasing T_{ox} above $\sim$800 °C. Comparison with mechanical-stress data for the Si/SiO_2 structure reveals close linear correlation with the average stress σ_{av} in the superficial SiO_2 film, so that $[P_b]$ is seen to decrease to $< 10^{10}$ cm^{-2}—*a* P_b-defect "free" interface—along with σ_{av} for $T_{ox} \rightarrow 1150$ °C. The underlying physical mechanism is global structure relaxation of the SiO_2 layer initiating at $\sim$800 °C, gradually reducing the need for intrinsic P_b generation to account for lattice mismatch. Other distinct variations in the P_b resonance also testify to this stress release effect such as the decrease in $g_{\parallel}$, linewidth narrowing, and change in line-shape symmetry. Line-shape simulations indicate that these effects result from the existence in the $T_{ox} < 800$ °C range of a variation of $\sigma_{g_{\parallel}} = 0.000\,32$ in $g_{\parallel}$, which strongly narrows upon enhancing T_{ox}. The drop in $g_{\parallel}$ refers to an average backward relaxation (over $\approx$0.13 Å) of the defect Si atoms to a more planar structure (less *s*-like hybridization), attendant with a downward shift of the P_b energy-level distribution over about 0.27 eV. An intrinsic defect, termed the *EX* center, is observed by ESR in as-oxidized Si oxide films.

I. INTRODUCTION

The Si/SiO_2 structure is still the basic ingredient in current metal-oxide-semiconductor (MOS) devices. Much of this success has resulted from such factors as the ease of fabrication, the superb quality of thermal Si oxide, and its perfect growth-inherent adhesion to the crystalline Si (*c*-Si) substrate. The trend to ever smaller devices with thin gate oxides (now entering the sub-100-Å region) in very-large-scale integration (VLSI) technology faces an ever-growing relative importance of the nonscaling Si/SiO_2 transition regions. This, obviously, puts an increasing burden on the thin SiO_2 layers, and exceedingly so on the electrical quality of crucial interfaces. For one, it is known that device performance may strongly be degraded by defect generation[1] as a result of stressing thin oxides and Si/SiO_2 interface regions by nonscaling electric fields.

But while the reliability of the Si/SiO_2 entity in relation to MOS devices was well recognized early on, much of its vulnerability results from the interface region where it is accepted that defects are naturally generated to account for interfacial stress. The latter incorporates both intrinsic stress resulting from structural mismatch and thermal shear stress. The defects, at room temperature, lead to electrical fast interface states (density D_{it}), with an energy distribution in the Si band gap, which behave as trapping and recombination centers.[2] This has evoked intense research into the structural identification of these defects ever since the incorporation of the Si/SiO_2 entity as a major constituent of successful devices (see, e.g., Refs. 2–7). And while not all defects in the Si/SiO_2 structure will contribute to direct current degradation, information on whatever kind of defect is important, as they may all lead to the untimely failure of refined chips.

The most structurally useful information about defects in Si/SiO_2 has come from analysis of *g* matrices and ^{29}Si hyperfine (hf) data (see, e.g., Refs. 6 and 7) supplied by electron spin resonance (ESR), albeit the application of the technique is restricted to those defects in a spin-active (paramagnetic) state. This, however, has generally not been a severe restriction, as initially diamagnetic defects may often be altered by ionizing events[8] and H diffusion.[3,4,9]

The main Si/SiO_2 interface defect has been characterized[4–6,7,10] as $Si_3 \equiv Si^0$, that is, a trivalently bonded Si atom at the Si surface of the Si/SiO_2 interface with the unpaired electron localized about 80% in an $sp^3_{[111]}$-like hybrid protruding into a microvoid in the oxide. It has C_{3v} symmetry and is the only interface defect, denoted as P_b, so far observed in (111)Si/SiO_2. At the (100)Si/SiO_2 interface, however, two defects, denoted as P_{b0} and P_{b1}, have been observed[5,7,11] by ESR, where P_{b0} has initially been interpreted as the (100) counterpart of P_b—an assignment that is currently under much debate.[12,13] A noteworthy observation is that in (111)Si/SiO_2 only the $[111]P_b$ species with an unpaired hybrid $\perp$(111)Si/SiO_2 interface occurs.[5,14] The other types—in short, called the 19° P_b centers—with the unpaired orbital along one of the "equivalent" directions $[\bar{1}11]$, $[1\bar{1}1]$, or $[11\bar{1}]$, are

not observed in conventional state-of-the-art Si/SiO_2 structures.[15]

Electric-field-controlled ESR in combination with capacitance-voltage (C-V) observations,[16–18] deep-level transient spectroscopy[19] (DLTS), and photoionization thresholds determinations[20] has led to a quantitative correlation of the P_b defect with a fast interface trap. Two peaks in the density of interface states within the forbidden energy gap at levels 0.3 and 0.85 eV above the valence band were shown to correspond well with the $(+/0)$ and $(0/-)$ transition levels of the P_b defect. This clearly demonstrates the amphoteric nature of P_b (effective correlation energy ≈ 0.55 eV) and the defect is found[17,18] to account for 50–100 % of all electrically active interface states.

An important technological aspect is that the thermochemical properties of P_b appear dominated[7,21–25] by interaction with H, an effect that has early on been recognized[21,22] from the passivation kinetics of electrically active interface traps. And, in fact, an elegant unified model[23] for the P_b hydrogenation chemistry has recently resulted from detailed ESR analysis of $(111)Si/SiO_2$ subject to H passivating and depassivating thermal steps. In the range 230–260 °C, passivation of P_b is found to proceed by the reaction

$$Si_3{\equiv}Si^0+H_2 \rightarrow Si_3{\equiv}SiH+H \ , \tag{1}$$

with an activation energy $E_a \approx 1.66$ eV, while the dissociation step, studied in the range 500–595 °C, is represented by the reaction

$$Si_3{\equiv}SiH \rightarrow Si_3{\equiv}Si^0+H \ , \tag{2}$$

characterized by $E_a \approx 2.56$ eV. Admirable in this interaction scheme is that the combination of both reactions simply yields the dissociation of the H_2 molecule and a net $E_a \approx 4.22$ eV, reassuringly in agreement with the textbook value of 4.52 eV for dissociation *in vacuo*. Also interesting is that the reverse reactions of (1) and (2) proceed with essentially no energy barriers, even at cryogenic temperature (T), the sole controlling factor being the availability of atomic hydrogen. This fact, as embedded in reaction (1), serves as a key ingredient in a clever H_2-based model recently proposed[26] to unify all experimental knowledge about radiation sensitivity and H exposure of the Si/SiO_2 entity in relation with the interface state dynamics. This model is thus in agreement with the interpretation of the thermochemical properties of interface defects when postulating hydrogen as the basic chemical agent in radiation kinetics of interface states. It is likely to constitute a breakthrough in the basic comprehension of the enigmatic radiation hardness of Si-based MOS devices. Much of the strength of this model results from the fact that it combines the ESR-monitored annealing behavior of pertinent species in the Si/SiO_2 structure [i.e., H^0, OH moieties, and self-trapped holes (STH's)] with H-related interface trap formation.

The recent stream of information on H incorporation is, to say the least, overwhelming, apparently indicating that our understanding of the role of H in the Si/SiO_2 structure is coming of age. In hindsight then, the dominant role of H proclaimed in interface state kinetics may perhaps not appear too surprising in light of the fact that significant interface trap alterations may occur at cryogenic T's, where atomic hydrogen is the only species of any type known that may diffuse sufficiently.

It is evident that the full understanding of interface trap density behavior over the various processing steps does require a basic knowledge of H kinetics in the Si/SiO_2 structure. But this, obviously, is only part of the matter. Equally important is the knowledge at the onset, that is, before any passivation has occurred, of all physical entities (defects) that may potentially lead to electrically active interface states. As the dominant role of P_b defects is well recognized in this respect [at least for the $(111)Si/SiO_2$ structure], a basic quantity is the intrinsic density of all P_b entities $[P_b^*] \equiv [P_b]+[HP_b]+[XP_b]$, including both ESR-active (P_b) defects and centers passivated by H (HP_b) or any other means (XP_b). The pristine number $[P_b^*]$ obviously plays a major role in H kinetics as borne out by reactions (1) and (2). More fundamental, perhaps, is that it might incorporate vital information about the intrinsic Si/SiO_2 structure—the structure ideally grown in pure O_2 ambient, in absence of any other chemical species. The unveiling of the atomic structure of that particular interface is still a main goal of the fundamental research on Si/SiO_2.

Identification of interface defects (and intrinsic defects in the SiO_2 layer, in general) may also add considerably to our understanding of interface structure and how thermal oxidation proceeds—topics that have evoked large theoretical efforts. Over the many years, numerous oxidation models have been forwarded that have led to a reliable description of oxidation rates (see, e.g., Refs. 27 and 28, and overviews in Refs. 29 and 30). These efforts, though, have apparently been most successful for the description of thicker oxides ($d_{ox} \geq 100$ Å), the thin region still attracting much theoretical and experimental interest.[29,31] Very pertinent in this respect is the recently advanced data inferring the existence of a dynamic reactive layer, about 1–2 nm thick, separating the c-Si substrate and superficial a-SiO_2 layer. The analysis of the physicochemical nature of this near-interfacial SiO_x layer is an active area of research, supported by various sophisticated experimental techniques (see Ref. 29 for an overview). The act of oxidation of Si, that is, the conversion of arriving interstitial oxygen molecules into network oxygens, is admitted to occur in this SiO_x layer, thus operating as the major delimiter of the various oxidation regimes the growing SiO_2 layer passes through. And, if present, there is no doubt that this layer, by its nature, will coestablish the kind of interface structure intrinsically grown. Other results point to the significance of microvoids[32] and Si inclusions[33]—perhaps inherent parts of the reactive layer—at the Si/SiO_2 interface.

The passivation of defects by H, either intentionally or not, has thus turned into a main device topic (cf. postoxidation annealing in forming gas). The present work intends to isolate the H-passivating factor with a view to determine the intrinsic P_b^* density. The reproducible thermal H passivation-depassivation method[9,25] is fully

exploited to maximize the number of spin-active P_b's at the (111)Si/SiO_2 interface, using high-sensitivity low-T ESR as the diagnostic tool. If, as likely, H is the major passivating agent in standard oxidation setups, the post-dehydrogenation P_b density should closely approach $[P_b^*]$. This then has allowed us to map the evolution of $[P_b^*]$ and ESR signal characteristics with varying oxidation parameters and temperature T_{ox} ranging from 22 to 1140 °C. A useful result this hopefully leads to is the assignment by ESR of the T_{ox} window intrinsically leading to the lowest $[P_b^*]$.

II. EXPERIMENTAL DETAILS

A. Samples

Samples having a 2×9 mm^2 (111) face, with their 9-mm edge along a $[11\bar{2}]$ direction, were fabricated from a commercial Czochralski-grown p-type Si wafer (B-doped, ≈10 Ω cm). Both (111) faces of this "mother" wafer were cupric-ion electrochemically polished to optical flatness, resulting in a final thickness of 117 ± 16 μm. Typically 13–15 slices were stacked to enhance the effective sample surface in the ESR cavity.

B. Thermal treatments

As it was aimed to conduct a comparative study of the Si/SiO_2 interface properties over a broad T_{ox} range, attention was paid to preclean samples identically prior to each oxidation procedure. Except for a specific set of samples, that precleaning procedure included a standard RCA-type cleaning,[34] as described elsewhere,[35] followed by thorough rinsings in high-purity H_2O ($\rho\geq18$ MΩ cm) and MOS-grade acetone. The slices were then quickly transferred (typically within 2 min) into the oven insert upon which thermal oxidation was initiated. This was carried out in a conventional resistance-heated furnace foreseen with a double-walled silica tube with an inner diameter of about 35 mm and about 35 cm long. It has exclusively been used for high-purity Si processing and is readily evacuated to below 2×10^{-7} Torr by a turbomolecular pump. This high-vacuum laboratory setup was regularly checked to be He leak tight to better than 10^{-10} Torr liter/s, and processing gas composition was continuously monitored by a quadrupole mass spectrometer. For purposes of fast heating or cooling, the oven could be transpositioned relative to the silica tube.

The quartz sample holder in the silica tube was a high-purity (Heralux quality) U shape foreseen with pairwise-positioned slits. It has been designed in such a way as to mount all sample slices close together (within an area <1.5 cm^2), yet well separated, with a minimum of contact area between samples and the holder. The (111) sample faces were thus at all times fully exposed to the ambient in the silica tube during thermal processing.

Two types of thermal treatments were standardly applied: First, thermal oxidation in the range 207–1140 °C for times t_{ox} ranging from 122 to 142 min in flowing dry O_2 (99.999% pure; 1.1 atm) at a pressure $p_{ox}\approx1.1$ atm. The oxidation was a crucial step and care was taken to assure that T_{ox} was the only changing parameter over the various, otherwise identical, oxidation steps performed. Second, after a first ESR analysis of the as-oxidized samples and subsequent appropriate cleaning, they were reintroduced into the furnace to submit them to thermal degassing. This implied heating at $T_{dh}=790\pm5$ °C for times $t_{dh}=60-70$ min in a $\leq2\times10^{-7}$-Torr vacuum, for all samples identically. As it is believed that the mere effect of this treatment is the liberation of H from the Si/SiO_2 structure, it is referred to as "dehydrogenation." Inlet and outlet ports of the silica insert were properly "guarded" by liquid-N_2 (or slightly higher T) baffles during all thermal cycling.

It should be noted that the way chosen to explore the specified oxidation range is isochronal (~2 h at temperature) oxidation at each T_{ox}, resulting in a large spread of oxide thicknesses. This is evidenced in Fig. 1, where the typical dry oxide film thickness d_{ox} grown in 2 h on (111)Si, as derived from Refs. 27 and 28 is plotted versus T_{ox}. It is seen that d_{ox} starts to increase, almost exponentially, above $T_{ox}\approx720$ °C, while the thickness remains effectively below 40 Å for all $T_{ox}<700$ °C. Obviously, another approach could have preferred to grow films of equal thickness at each T_{ox}. But this is hardly tenable; growing a film of some substantial thickness, say 100 Å, in a reasonable time is not realizable at low T_{ox}, while growing such a thin film at high T_{ox} (>1100 °C) appears equally difficult in view of the fast oxidation rate. Hence the former approach has been preferred.

There is a particular remark about the fact that the degassing cycle at 790 °C has been applied to all samples identically. Samples that have been oxidized at $T_{ox}<790$ °C were thus submitted to a dehydrogenation temperature *exceeding* their growth temperature, unlike the other samples. The possibility that this might ensue a cooperative relaxation effect of the oxide on the first suite of samples should be recalled when addressing any eventual variations of $[P_b]$ as a function of T_{ox} (*vide infra*).

Beside the above variation of T_{ox} for the main set of samples, some additional parameters were altered in

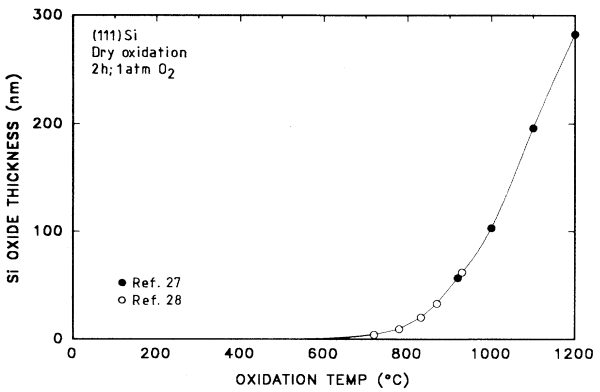

FIG. 1. Thickness of oxide layers grown in dry O_2 in ≈2 h on (111)Si at various temperatures. The data points were taken from Refs. 27 (filled circles) and 28 (open circles), while the solid line represents a parabolic fit.

some other preparations with a view to trace their influence on the P_b system. This incorporates variation of p_{ox} from 1.5×10^{-5} to 840 Torr, native oxidation, and three preoxidation heating and postoxidation cooling ambients, that is, either vacuum ($\leq 2\times10^{-7}$ Torr), O_2 or N_2 flow.

Furthermore, a second type of substrate precleaning was tested. As a first step, a sacrificial oxide was grown at $\approx$930 °C for about 2 h along the standard scenario outlined above. The samples were then submerged in a 5% HF aqueous solution [HF(49%):H_2O; 1:9; etch rate $\approx$4 Å/s] sufficiently long as to remove the oxide layer. But not excessively longer, however, as indicated by the hydrophobic nature of the Si surfaces. This results in pristine Si surfaces protectively covered predominantly by a single layer of Si monohydride.[36] Hereupon then was initiated the standard thermal oxidation. These samples are referred to as HF *cleaned*.

Some samples were submitted to a third thermal step following the ESR analysis after dehydrogenation. This implied hydrogenation in 99.9999%-pure H_2 ($p\approx1.1$ atm) at 253–353 °C for 10–20 min, resulting in (partial) passivation of the P_b centers (HP_b entities). Hydrogenation and dehydrogenation steps may be freely sequenced. It has indeed been shown before[25] that this non-*in situ* H cycling in combination with intermediate appropriate cleaning in acetone constitutes a fully reproducible P_b passivation scheme. It is, in fact, an adequate probe for tuning the ESR-active P_b density, which one can take advantage of for studying some particular P_b characteristics, e.g., reducing dipole-dipole (DD) interaction[25] between P_b's, or, attendantly, monitoring the saturation sensitivity.

There are of course many possible ways to initiate or abort the oxidation step, and various postoxidation annealings can be considered. And indeed, in paving the way to high-quality semiconductor processing, these "boundary" treatments have been the subject of intense research, the prevention of interface trap formation at crucial interfaces having been a main goal. Best known, perhaps, in this respect is the benign influence of the now reasonably well understood postoxidation annealing in forming gas ($\sim$30% H_2; 70% N_2) at moderate T's ($\approx$450 °C). The impact of other preoxidation or postoxidation conditions has appeared less drastic. In the current research, however, we remained with one (common) fixed oxidation scheme for the major part of the preparations. This, of course, was to avoid any unnecessary interference with the influence of those parameters envisioned. In the chosen procedure, after having inserted the slices into the silica tube, the latter was evacuated to below $\sim10^{-2}$ Torr and rinsed with N_2 (99.9999% pure; $\sim$1.1 atm), at least three times in sequence. This N_2 rinsing ended with evacuating the tube to below 2×10^{-7} Torr, whereupon the tube was introduced into the oven, preset at the desired T_{ox}. About 10 min were then allowed for thermal equilibration between the low-mass samples and the oven, a process occurring by virtue of heat exchange due to thermal radiation. Thermal oxidation was abruptly initiated by opening the O_2 blocking valve. After the desired time, this was quickly terminated by offsetting the furnace from the silica tube, thus allowing the samples to cool to room temperature ($\approx$22 °C) in about 25 min; typical time-temperature heating and cooling profiles are shown in Fig. 2.

The furnace temperature was microprocessor controlled using Cr-Al thermocouples (type *K*) enclosed in silica tubes as T sensors of the crucial oven and sample space; the typical accuracy reached at T_{ox} is $\approx$0.5%.

While numerous oxidations have been carried out, effectively only two ESR sample stacks, each comprising 14 2×9-mm^2 slices, were processed. After having carried out a first research cycle, that is, all desired thermal steps and ESR analysis, the (111) sample surfaces were reset to a virgin state by etching off the oxide in aqueous HF (as described above) and submitting them to either of the two precleaning procedures mentioned. Obviously, this scenario has some advantages over the case where each oxidation cycle starts from a different set of Si slices, such as identical basic Si and sample surface for all oxidations.

C. ESR spectrometry

ESR observations were made at 4.3 K using a *K*-band ($\approx$20.2 GHz) homodyne spectrometer, equipped with a balanced mixer microwave bridge, in absorption mode under conditions of adiabatic slow passage. The general spectrometer buildup and performance as well as the reason why liquid-He observational temperatures have been preferred has been outlined previously.[25] However, the strong saturability of the P_b defect at these low T's imposed to restrict the microwave power P_μ incident on the TE_{011} cylindrical cavity of loaded quality factor $Q_L\approx13\,000$–$16\,000$ to below 1 nW, typically. Phase-sensitive detection was achieved by sinusoidal modulation at 100–150 kHz of the applied magnetic induction **B**, resulting in the recording of the absorption-derivative spectra $dP_{\mu a}/dB$, where $P_{\mu a}$ represents the absorbed microwave power. All measurements were carried out with

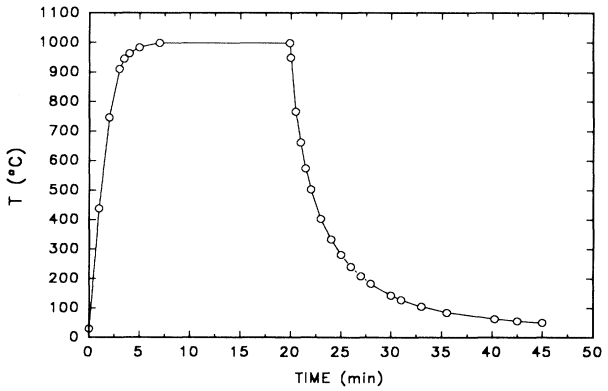

FIG. 2. Temperature-time profile picturing the heating up and cooling cycles of the sample space inside the silica oven insert. At time $t=0$, the furnace, preset at 1000 °C, was quickly positioned over the fixed silica tube, while at $t=20$ min, the oven is abruptly offset from the tube. The solid line is a guide to the eye.

$\mathbf{B}\perp(111)\mathrm{Si/SiO_2}$ interface to optimize sensitivity.[10]

Spin densities and g values were accurately determined along the procedures extensively outlined elsewhere.[25] Essentially, spin densities were measured relative to an isotropic reference signal by comparing the intensity I (area under the absorption curve) of both signals as obtained by double numerical integration of the respective $dP_{\mu a}/dB$ spectra *recorded in one trace.* The spin standard was a small amount of c-Si:P powder, doped to $[P]=1.7\times10^{18}$ cm^{-3}, which is routinely attached to the $\mathrm{Si/SiO_2}$ sample bundle at all times during ESR observation. The single exchange-narrowed P-donor signal of this reference sample has been minutely calibrated against the primary standard $\mathrm{Al_2O_3:Cr^{3+}}$, known to an accuracy of $\pm1\%$. It is estimated that the obtained absolute accuracy of P_b density is typically $\pm10\%$, while a relative accuracy of better than 5% may have been reached when comparing $[P_b]$ for one sample bundle over various thermal cyclings.

The integration of $dP_{\mu a}/dB$ P_b spectra merits special attention. It has indeed been shown previously that variations in $[P_b]$ may be accompanied by significant alterations in the line shape due to the varying impact of DD interactions within the effectively two-dimensional dilute spin system.[25] The general trend is that progressively more oscillator strength shifts to wing features (fine structure) with increasing $[P_b]$, thus dictating appropriate scaling of the integration field range to enclose a sufficient amount of signal. This effect has been accounted for by fixing the integration range for all P_b signals measured to a width of ~53 G, centered at the P_b zero crossing field B_0, well adjusted to the highest $[P_b]$ values encountered.

The comounted Si:P spin standard simultaneously serves as an excellent, isotropic g marker. Its g value, given at 4.3 K as $1.998\,69\pm0.000\,02$, has been calibrated against the stable LiF:Li g standard.[37] This allows us, again by relying on the relative method, to obtain an accuracy of $\pm0.000\,03$ for measured g values.

III. EXPERIMENTAL RESULTS AND DISCUSSION

A. Spin densities

Illustrated in Fig. 3(b) is the variation of $[P_b]$ as a function of T_{ox} for RCA-precleaned $\mathrm{Si/SiO_2}$ structures in the as-oxidized state (filled symbols) and after subsequent exhaustive dehydrogenation at 790 °C (unfilled symbols) along the procedure outlined. The exhaustive[38] nature of this P_b ESR activation is evident from recent detailed studies of the HP_b dissociation kinetics,[39] and, though somewhat indirectly, it is also clear from[22] the evolution of D_{it} as a function of T_{dh}. If necessary, we have further substantiated this conclusion by extending t_{dh} from ~60 min up to 150 min, without any effect, however, on the ultimate $[P_b]$. The increase of T_{dh} to 835 °C also did not lead to any additional enhancement of $[P_b]$. So, it is henceforth assumed that $[P_b^*]=[P_b]_{dh}$, the density observed after appropriate degassing, although, notationally, we shall keep using $[P_b]$ for reasons of simplicity.

A general observation is that all as-oxidized $[P_b]$ data—except, apparently, those at the extreme T_{ox} ends—situate in the range $(4-5)\times10^{12}$ cm^{-2}, in agreement with previous observations.[4,5,11,40] But it should be noticed that $[P_b]$ decreases[41] for $T_{ox}>1000$ °C, down to $(1.9\pm0.2)\times10^{12}$ cm^{-2} at ≈1135 °C, while some increase may occur for $T_{ox}\approx22$ °C.

Of main interest is the dehydrogenated-samples data [unfilled symbols in Fig. 3(b)], and various features merit attention. First, note can be taken of the significant overall increase in $[P_b]$ upon vacuum treatment[42]—generally in excess of a factor of 2 in comparison with the as-oxidized values. Second, the $[P_b]$ vs T_{ox} plot exhibits various trends. As indicated by the solid line, drawn to guide the eye, $[P_b]$ decreases drastically at the high-T_{ox} end, the trend suggesting $[P_b]\rightarrow<10^{10}$ cm^{-2} (the detec-

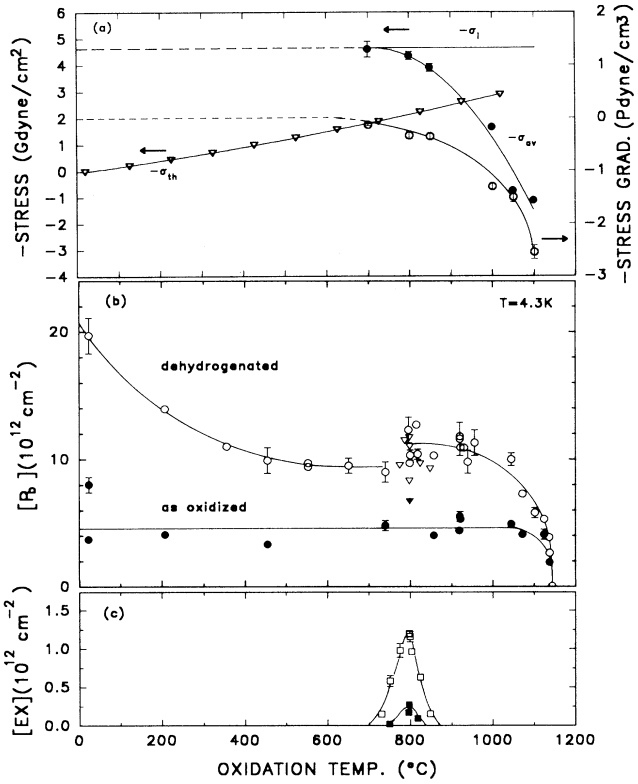

FIG. 3. Various stress quantities (a) identified in the superficial SiO_2 layer of Si/SiO_2 structures. The data points plotted for the average and intrinsic SiO_2 film stress (filled circles) and near-interfacial stress gradient (open circles) come from Refs. 51 and 52, where the latter values represent the slopes of the measured stress vs d_{ox} curves for $d_{ox}<d_{ox}^c$ (see also Fig. 8). The thermal stress data were obtained from relation (4) using the thermal expansion data presented in Ref. 46. (b) The P_b density observed on RCA-cleaned (111)Si/SiO_2 oxidized for about 2 h in 1.1 atm O_2 at various T_{ox}'s both for the as-oxidized state (●) and after subsequent exhaustive dehydrogenation (○) at 790 °C for ≈1 h in vacuum. The triangles refer to HF preoxidation cleaning. Observed in the SiO_2 layers is a defect, the *EX* center, of which the density observed after exhaustive dehydrogenation is displayed in (c) both for HF (□) and RCA (■) precleaning. The solid lines through the σ_{av} and stress gradient data represent least-squares parabolic fits, while the other lines are only meant to guide the eye.

tion limit[25]) for $T_{ox} \rightarrow 1150\,^{\circ}C$. At the low-$T_{ox}$ end, in contrast, the P_b density increases monotonically to reach a value of $(19.7 \pm 1.4) \times 10^{12}$ cm^{-2} at $T_{ox} \approx 23\,^{\circ}C$. The noteworthy general trend, though, is that the $[P_b]$ data change little ($<20\%$) over the broad T_{ox} range extending from ≈ 200 to about $1000\,^{\circ}C$. But clearly, something appears to occur around $800\,^{\circ}C$, at which T_{ox} the scatter of the data has increased. This could refer either to a transition from an oxidation regime dominated by electric-field dependent transport (cf. the Cabrerra-Mott model) to one solely governed by concentration gradients of crucial species,[30] or simply to enhanced sensitivity of the P_b generation to subtle preoxidation Si surface conditions. Additionally it should be recalled, though, that whatever the oxidation temperature applied, all samples were identically vacuum treated at $\approx 790\,^{\circ}C$. This means that all samples grown at $T_{ox} > 790\,^{\circ}C$ were never submitted to a higher temperature than their oxidation temperature. The bearing of this should be recalled when interpreting the data. For one, vacuum annealing at $790\,^{\circ}C$ of Si/SiO_2 structures grown at substantially lower T_{ox} might have resulted in an additional global interface relaxation. So, it seems advisable to treat the $[P_b]$ results in Fig. 3 as two sets of data, separated by the $T_{ox} = 790\,^{\circ}C$ boundary.

Figure 3(b) has additionally included some $[P_b]$ results (unfilled triangles) on HF-cleaned slices. Although these data span only the window $T_{ox} = 700-850\,^{\circ}C$, their general trend is of being slightly lower than their RCA counterparts. This shows that changing precleaning conditions may slightly affect the P_b density, at least for oxidations in the range $T_{ox} = 700-850\,^{\circ}C$ for about 2 h. As this is likely to depend on d_{ox}, it is useful to mention that oxidation at $800\,^{\circ}C$ in dry O_2 (1.1 atm) for about 130 min produces a ~ 115-Å-thick Si oxide layer (cf. Fig. 1).

B. Signal from SiO_2

The main motivation that has prompted us to explore the HF-precleaning procedure is a result pictured in Fig. 3(c). This shows the areal spin density versus T_{ox} of an observed defect, termed the *EX* defect. A typical ESR spectrum of this defect, observed on a HF-cleaned sample, is depicted in Fig. 4. It is seen that the spectrum consists of a dominant central line of $\Delta B_{pp} = 1.0 \pm 0.1$ G, centered at $g = 2.002\,46 \pm 0.000\,03$ amid a weak doublet of 16.1 ± 0.1 G splitting. Typifying the central line is its symmetric line shape (i.e., no apparent glass-powder effects) of Voigt shape, characterized by the line-shape factor $\kappa \equiv I_c / A_{pp} (\Delta B_{pp})^2 = 1.8 \pm 0.1$, where I_c represents the central signal intensity and $2A_{pp}$ the peak-to-peak height of the first-derivative signal. (For clarity, we recall that the line-shape factor equals 1.03 and 3.63 for the familiar Gaussian and Lorentzian curves, respectively. The Voigt profile, being a convolution of these shapes, is thus expected to fall in the range $1.03 \leq \kappa \leq 3.63$.) Another unique feature is that its g value (zero crossing) is found to be fully isotropic, that is, no g shift is observed for **B** tilting from $\|[111]$ [$\mathbf{B} \perp (111)Si/SiO_2$ interface] towards $\perp[111]$. And no T dependence of g, ΔB_{pp}, and the line shape is observed in the range 4.3–25 K. The width of each doublet line, quantified as ≈ 1.2 G, is close to the width of the central line.

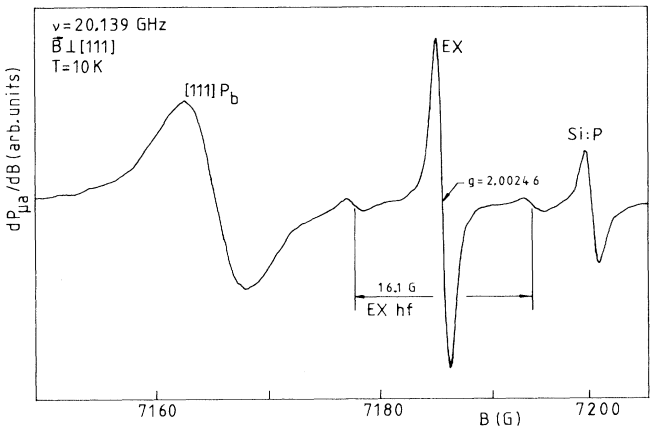

FIG. 4. A first-derivative ESR spectrum observed at 10 K for $\mathbf{B} \| (111)Si/SiO_2$ interface on HF-precleaned $(111)Si/SiO_2$ grown at $800\,^{\circ}C$ for 2 h and subsequently dehydrogenated. The isotropic central *EX* signal amid its attendant characteristic doublet is indicated. Note that for this **B** orientation, the P_b defect resonates at $g = 2.0088$. The Si:P signal stems from a Si:P powder reference sample of $g(4.3\text{ K}) = 1.998\,69 \pm 0.000\,02$.

An intriguing aspect of this spectrum is that it appears only to be generated in the $(111)Si/SiO_2$ structure, at least in its ESR-active state, after oxidation in the range $T_{ox} = 700-850\,^{\circ}C$, as illustrated in Fig. 3(c); the maximum signal of $\approx 1.2 \times 10^{12}$ cm^{-2} $S = \frac{1}{2}$ spins is observed for $T_{ox} \approx 800\,^{\circ}C$. Noteworthy also is that the signal intensity is low for all RCA-cleaned samples (filled symbols), but increases significantly if starting from HF-cleaned substrates (open symbols); at $T_{ox} \approx 800\,^{\circ}C$, HF-precleaning results in a 5 times larger *EX* signal than RCA cleaning, thus bearing out the importance of the preoxidation surface condition. Sequential etch back in diluted HF [HF(49%):H_2O; 1:9 (by volume)] of a sample that had grown on a 11.4 ± 1.2-nm-thick Si oxide revealed the *EX* defect to be localized in the top half of the oxide layer. It is important to add that during this etching, the copresent P_b signal remains unaffected, substantiating that *EX*, unlike P_b, is not an Si/SiO_2 interface center.

Another typical property of the *EX* center is that it appears affected by interaction with H in much the same way as P_b. Indeed, while the *EX* center is well observed in *as-grown* $(111)Si/SiO_2$ samples, its intensity was found to increase significantly—up to a factor of 4—upon vacuum annealing at $\sim 790\,^{\circ}C$ along the procedure outlined [and they are the latter values that are shown in Fig. 3(c)]. Longer vacuum treatment had no effect. Subsequent hydrogenation then in 1.1 atm H_2 at $\sim 360\,^{\circ}C$ for about 21 min totally bleached the ESR signal, but it fully reappeared after the usual vacuum anneal. It thus follows that, like the P_b center, the *ex situ* H passivation-depassivation sequence constitutes a highly reproducible procedure for the *EX* center, too, leaving the total intrinsic density $[EX^*]$, including both ESR-active and passivated centers initially present, unaltered.

An analysis of the *EX* center has been presented else-

where[43] concluding that it is an *intrinsic* defect—that is, not related to unwanted impurities—that has apparently not been observed before. It furthermore appears to be the first defect intrinsically generated in *as-grown* SiO_2, i.e., not created as a result of irradiation with some energetic particle, in contrast with the well-known E' center.[44] It has further been evidenced that the EX doublet results from interaction of the unpaired spin with ^{29}Si nuclei ($I=\frac{1}{2}$; 4.27% naturally abundant) at three equivalent neighboring Si sites. The general conclusion is that it regards an unpaired electron spin ($S=\frac{1}{2}$) occupying an effectively nearly pure s state—not primarily localized at one Si site—and exchanging a ^{29}Si superhyperfine interaction with three equivalent neighboring Si sites. A possible microscopic model is a hole trapped in an SiO_4-vacancy-type intrinsic defect.

We are thus confronted with the finding that thermal oxidation in dry 1.1 atm O_2 at $T_{ox}=700-850\,^{\circ}C$ results in the natural incorporation of up to 1.2×10^{12} cm^{-2} intrinsic ESR-active defects in thin (50–140 Å) as-grown SiO_2 films. And when referring to the application of the Si/SiO_2 entity in semiconductor devices, this is a somewhat alarming finding, in light of the likely charge trapping nature of these defects. The possible hazardous impact these defects may have on the quality of the omniapplied Si oxide provides sufficient stimulus for initiating a detailed investigation of the generation kinetics of the EX center. That information may be important in light of the steadily shrinking gate oxide thickness in crucial metal-oxide-semiconductor devices, entering the sub-100-Å region, for aimed 64-Mbit chips. But apart from this practical consideration, unveiling how such a defect is intrinsically generated during the oxidation process will be intriguing for our *fundamental* understanding of the a-SiO_2 structure.

To date, the defect has been observed only for $T_{ox}=700-850\,^{\circ}C$, at least in its ESR-active state. But a natural question follows as to whether it is also present in comparable amounts for oxidation outside the specified window—obviously then in a different (ESR-inactive) charge state—or whether it is then just not generated. Particularly fruitful in this respect may be the combination of ESR with ionizing radiation, able to change the charge state of otherwise chemically unaltered defects. Defect research has indeed benefited much from such symbiosis in the past.

C. Linewidth and g value

The P_b $g_{\parallel}$ data are depicted in Fig. 5(b). When focusing on the vacuum-treated samples (open symbols), a constant value $g=2.001\,44\pm0.000\,03$ appears to hold over the range $T_{ox}<700\,^{\circ}C$, but then g clearly tends to a minimum of $2.001\,36\pm0.000\,03$ at $T_{ox}\approx950\,^{\circ}C$, to increase somewhat for higher temperatures. This trend is also apparent from the as-prepared results, albeit somewhat less convincingly. Both sets of data seem to coincide (apart perhaps from the room-temperature values), indicating that the postoxidation dehydrogenation treatment did not much affect the $g_{\parallel}$ magnitude. While the overall change may appear small, there is thus a clear evolution in P_b's g value with T_{ox}, in contrast with previous belief. This then, by the nature of the interactions that induce shifts $\Delta g=g-g_{fe}$ away from the free-electron value $g_{fe}=2.002\,319$, may point to a dependence of the mean P_b core defect structure on T_{ox}.

Next is considered the peak-to-peak linewidth ΔB_{pp} of the unsaturated P_b signal, plotted in Fig. 5(a). A first glimpse at these data makes it clear that they mirror in some sense the $g_{\parallel}$ vs T_{ox} results shown in Fig. 5(b). For the dehydrogenated structures, ΔB_{pp} appears constant with a mean value of 2.6 ± 0.15 for $T_{ox}<700\,^{\circ}C$, the width then tending to a minimum of 1.9 ± 0.1 G for $T_{ox}\rightarrow900\,^{\circ}C$. And, also similar to the g data, this pattern is closely reproduced by the as-oxidized sample set. It should be noted, though, that the latter values are generally slightly lower than their dehydrogenated counterparts, a fact that is expected from dipolar interactions between P_b's. Indeed, it has previously been reported[25] for $T_{ox}\approx929\,^{\circ}C$ that ΔB_{pp} increases from 1.69 ± 0.02 to 1.90 ± 0.02 G upon dehydrogenation of an as-grown P_b system due to enhanced dipolar broadening in the more intense spin system. But clearly then, when comparing Figs. 3(b) and 5(a), this ΔB_{pp} broadening upon dehydrogenation should be even more pronounced for the $T_{ox}<400\,^{\circ}C$ samples in view of the much enhanced $[P_b]$

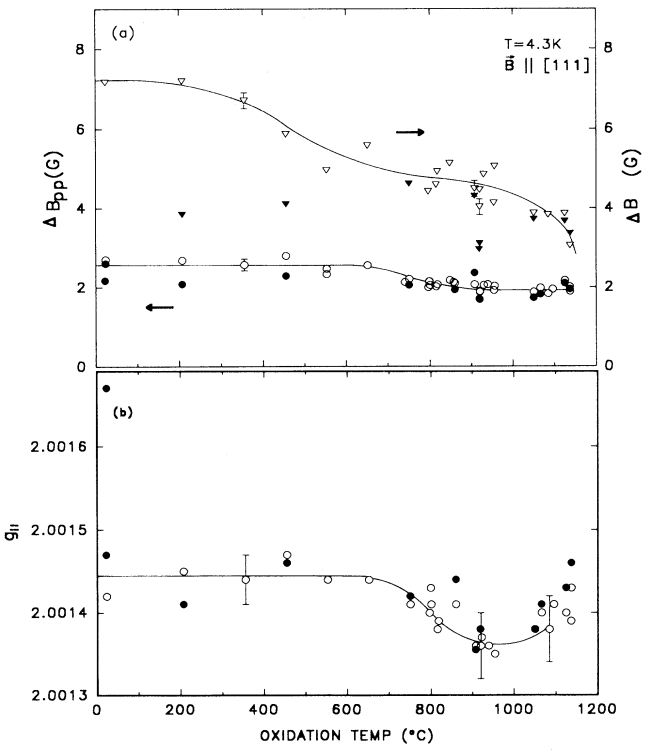

FIG. 5. Plot of the peak-to-peak width of the first-derivative spectrum, width at half height of the integral spectrum, and the g factor of P_b centers in (111)Si/SiO_2 structures measured at 4.3 K for $\mathbf{B}\perp(111)Si/SiO_2$ interface. All samples were RCA cleaned prior to oxidation in dry O_2 for ≈2 h. Filled and hollow symbols refer to the as-oxidized and exhaustively dehydrogenated state, respectively. The solid lines are guides to the eye.

as compared to the higher-T_{ox} samples, a trend that is not observed. For example, the linewidths of as-oxidized and degassed native oxide/Si structures are almost equal, while corresponding to significantly different P_b densities, i.e., $(4-8)\times10^{12}$ and $\approx2\times10^{13}$ cm^{-2}, respectively. This suggests the admixing of another line-broadening mechanism competing with dipolar interaction, with an attendant change in line shape.

Also plotted in Fig. 5(a) is the width at half height ΔB measured on the integral spectra, for comparative purposes. When first focusing on the dehydrogenated samples, a noteworthy observation is the significant increase in ΔB upon degassing in the low-T_{ox} (<500 °C) range, in contrast with the higher-T_{ox} region. This confirms the profound change in line shape. That this is indeed the case is pictured in Fig. 6, where the P_b signals observed at 4.3 K on $T_{ox}=23$ and 207 °C samples in the as-grown state and after subsequent vacuum annealing are compared. The general trend of the ΔB data is a monotonical decline with increasing T_{ox}, showing apparently little correlation with ΔB_{pp}, which must point to a changing line shape with varying T_{ox}. This is well affirmed by the plot of the line-shape factor in Fig. 7. The line-shape factor is seen to set off at a value of 7.0 ± 0.3 for

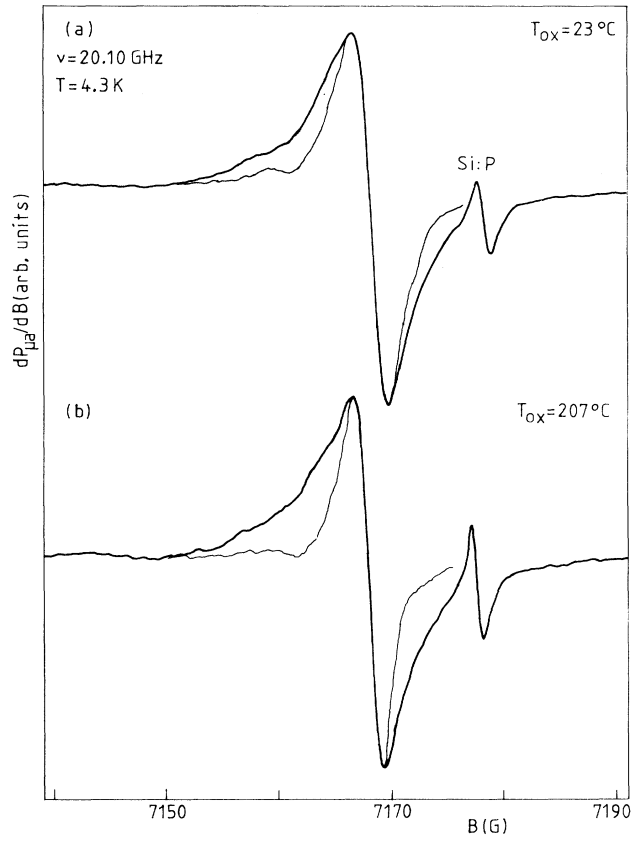

FIG. 6. Typical K-band P_b ESR spectra measured at 4.3 K on as-grown (thin line) and dehydrogenated (bold line) (111)Si/SiO_2 entities for $\mathbf{B}\perp$(111)Si/SiO_2 interface. A significant change in line shape is noticed upon degassing at ≈790 °C for about 1 h.

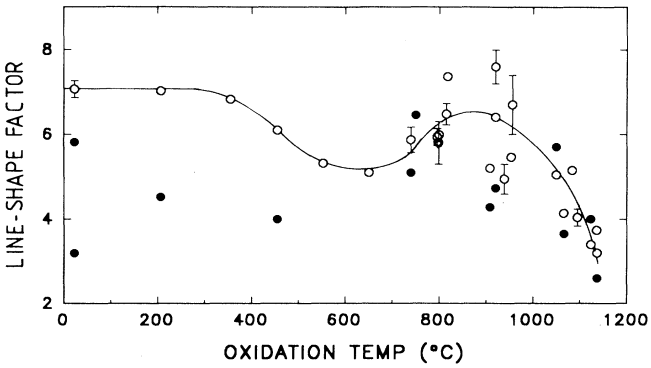

FIG. 7. Oxidation temperature dependence of the P_b line-shape factor, defined as $I/A_{pp}(\Delta B_{pp})^2$. Measurements were carried out at 4.3 K for $\mathbf{B}\perp$(111)Si/SiO_2 interface, both on as-oxidized (●) and subsequently dehydrogenated (○) (111)Si/SiO_2 entities. The solid line is a guide to the eye.

$T_{ox}<300$ °C, then goes through a minimum of 5.1 ± 0.3 at ~650 °C and declines quickly above ~1000 °C to reach an ultimate value of 3.5 ± 0.25 at $T_{ox}=1140$ °C.

The message from the κ data of as-grown samples, exhibiting increased scatter, is less clear. One can state, though, as the general trend, that they are smaller than the degassed sample values in the broad range $T_{ox}<1000$ °C, while both data sets merge at the high-T_{ox} end.

One might expect the existence of some correlation of κ with the linewidth, and since the latter incorporates a part due to dipolar broadening, possibly also with $[P_b]$. When focusing on the degassed samples, the κ and ΔB data indeed exhibit correlation, particularly regarding two aspects: they both remain constant in the range $T_{ox}<400$ °C, while both decline steeply above ~1000 °C. Note can be taken also of the close tracking of κ with $[P_b]$ [cf. Figs. 7 and 3(b)] for oxidation temperatures above ~400 °C. Hence, it may be concluded that for $T_{ox}>800$ °C, all three quantities ΔB, κ, and $[P_b]$ show close correlation in their dependence on T_{ox}.

IV. INTERPRETATION

A. P_b intensity

The P_b density–T_{ox} profile is analyzed with particular interest since it concerns here P_b defects *intrinsically* generated during conventional thermal oxidation (under widely applied conditions), as distinct from defects introduced by some form of postoxidation damaging.[8]

As alluded to in the Introduction, stress resulting from mismatch between the two dissimilar c-Si and a-SiO_2 layers is broadly accepted as the driving agent for P_b generation, *without the involvement of impurities.* But in a more refined approach, one may want to discriminate between various stress quantities: (1) *intrinsic interface stress* σ_i due to the difference in molar volume of both solids confronted at a single Si/SiO_2 interface plane, i.e., differences in bond length (Si-Si interatomic spacing is ~2.352 and 3.06 Å in c-Si and SiO_2, respectively), angles, and bond

densities, that prevent a perfect geometrical match; (2) *average stress* σ_{av} developing in the thickening oxide film; (3) *thermal expansion stress* σ_{th}, developing upon cooling to room temperature (RT) as a result of the difference in the thermal expansion coefficient α between a-SiO_2 [$\alpha_{SiO_2}=(0.50\pm0.06)\times10^{-6}$ K^{-1}, almost constant[45] within the range 300–800 K] and Si (α_{Si} increases monotonically[46] from 2.555×10^{-6} K^{-1} at 293 K to 4.41×10^{-6} K^{-1} at 1000 K). Little is known about which of the above stress components dominates P_b generation. One piece of information, though, has been obtained from the observation of large P_b densities ($>10^{12}$ cm^{-2}) in (111)Si/native oxide structures,[47,48] indicating the intrinsic stress to be dominant. Similar evidence comes from the ESR observation indicating that $[P_b]$ remains unchanged[19,49] in the range 4.2–300 K. But as no *in situ* ESR observations have so far been carried out at the actual temperature of oxidation, the influence of σ_{th} has as yet not been fully separated.

The present work addresses this issue by combining ESR results with previous work on stress analysis. And it is a fortunate fact that there has recently been carried out extensive research[50–53] on the dependence of stress in thermally grown SiO_2 on Si as a function of T_{ox} and d_{ox}. That comparison will be eased significantly by a concise summary of the main stress results. The latter were directly obtained from laser beam deflection measurements on p-type (111)Si wafers that, similar to the present ESR study, had also received an RCA preoxidation cleaning. All main stress components are *compressive* (negative) and *lateral* (parallel to the Si/SiO_2 interface plane), while the stress in the perpendicular direction is relatively weak.

The dependence on T_{ox} of the various stress components (see Refs. 51 and 52) has been synopsized in Fig. 3(a), where it should be added that the plotted σ_{av} data points (taken from Refs. 51 and 52) were read for the actual d_{ox} (cf. Fig. 1) grown in this work at each T_{ox} after 2 h (see also Fig. 8). It is seen from Fig. 3(a) that the intrinsic interface stress σ_i, that is, the stress in the thin SiO_2 film for $d_{ox}\to0$, is pinned at the value of $-(4.6\pm0.5)\times10^9$ dyn/cm^2 within the investigated T_{ox} range of 700–1100 °C. This constant and large, in magnitude, stress is seen as the embodiment of the mismatch between the molar volumes of Si and SiO_2, subject to the constraints imposed by almost complete chemical bonding at the Si/SiO_2 interface.

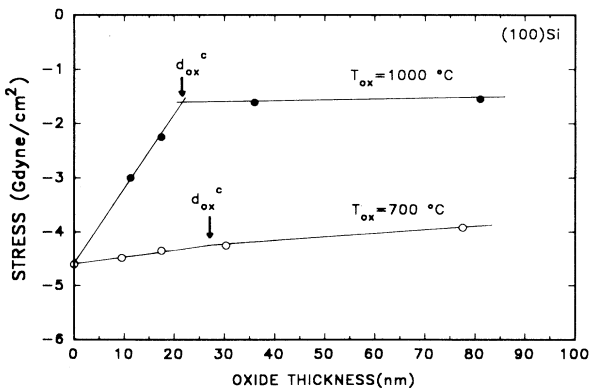

FIG. 8. Stress in superficial SiO_2 layers on Si as measured by the laser beam deflection technique [after Kobeda and Irene (Ref. 51)]. The crossing of the asymptotic lines defines for each T_{ox} a characteristic thickness d_{ox}^c at which both slopes merge fairly abruptly. Notice that an initially ($d_{ox}<d_{ox}^c$) larger slope implies a lower stress magnitude in the thick ($d_{ox}>d_{ox}^c$) range.

Also shown in Fig. 3(a) is the thermal stress calculated from the expression (see, e.g., Ref. 54)

$$\sigma_{th}=\int_{RT}^{T_{ox}}E'_{ox}(T)[\alpha_{ox}(T)-\alpha_{Si}(T)]dT\ , \tag{3}$$

applicable to a film negligibly thin compared to the substrate. Here, $E'_{ox}=E_{ox}/(1-\mu_{ox})$ is the generalized effective in-plane stress modulus, where E_{ox} and μ_{ox} represent Young's modulus and the Poisson ratio of the oxide film, respectively. E'_{ox} and α_{ox} are approximated by the T-independent values 8.0×10^{11} dyn/cm^2 (Ref. 55) and 0.50×10^{-6} K^{-1}, respectively, leading to

$$\sigma_{th}=E'_{ox}\left[\alpha_{ox}(T_{ox}-293)-\int_{293}^{T_{ox}}\alpha_{Si}(T)dT\right]\ , \tag{4}$$

where the second term on the right-hand side (rhs) is obtained from the compilation in Ref. 46.

The third quantity depicted in Fig. 3(a) is the average film stress, showing $|\sigma_{av}|$ ($=|\sigma_i|$ for $T_{ox}<700$ °C) to decline above $T_{ox}\approx700$ °C. This is clearly correlated with the thickening of the oxide layer grown in 2 h, which, effectively, sets in only above ≈700 °C (cf. Fig. 1). This is explained[51,52,56] by the fact that as the SiO_2 film grows by consumption of the Si substrate, part of the initially generated stress at the Si/SiO_2 interface is relieved into the bulk of the oxide layer by "viscous" motion[57] of SiO_2 away from the interface, resulting in a reduced average stress. That effect is seen to accelerate drastically with growing T_{ox}, the intrinsic stress apparently fully relaxing for $T_{ox}>1130$ °C for sufficiently thick oxides. Within the Maxwell viscoelastic model for a solid,[51,52,54] this increasing effect results from a drastic decrease in viscoelastic relaxation time τ. In effect, the stress data show that almost no viscoelastic relaxation can occur during film growth for $T_{ox}<800$ °C.

A fourth main observation from Fig. 3(a) is the existence of strong stress gradients in SiO_2 films in the immediate vicinity of the Si/SiO_2 interface, as inferred from[51,52] laser beam deflection data; these are corroborated by[58] the measurement of the Si-O bond-stretching frequency ν_{ir} by infrared (ir) spectroscopy. These gradients have been interpreted as the result of the unequal thermal history of the various oxide layers, simply referring to the fact that SiO_2 layers have benefited progressively longer from stress-relaxing annealing at the particular growth temperature according to their more remote position from the interface. The stress gradient in Fig. 3(a) is seen to decline (i.e., growing in magnitude) sharply above $T_{ox}>800$ °C, similar to the $|\sigma_{av}|$ data. To facilitate the understanding of the significance of this stress gradient in relation to the P_b properties, we have schematically reproduced in Fig. 8 two stress versus d_{ox} profiles as observed by Kobeda and Irene[51] on (111)Si/SiO_2 structures

oxidized at 700 and 1000 °C to different oxide thicknesses. Characteristic in this plot is the drop in $|\sigma_{av}|$ with increasing d_{ox}, a drop that gets more pronounced the higher T_{ox}, attendant with a strong increase in the near-interfacial stress gradient. As indicated in Fig. 8, the initial drop for $d_{ox} < 200$ Å may be approximated by a linear relationship, the fitted lines, as expected, converging to the interface stress σ_i value. It is the slope of these lines for $d_{ox} < 200$ Å that is taken as a measure for the near-interface stress gradient, plotted in Fig. 3(a). Figure 8 also illustrates that when the oxide film thickness exceeds a certain characteristic value d_{ox}^c, e.g., $d_{ox}^c \approx 220$ Å for $T_{ox} = 1000$ °C, the slope of the stress plots decreases drastically, the stress leveling at a value characteristic for each T_{ox}.

A noteworthy observation in Fig. 3(a) is that the σ_{av} vs T_{ox} plot is well mirrored by the stress gradient data. But this should not come as a surprise. Indeed, it is clear from Fig. 8 and related figures in Refs. 51 and 52 that the interfacial stress gradient shows a one-to-one relationship with the corresponding σ_{av} plateau value for $d_{ox} > d_{ox}^c$; that is, the decrease in $|\sigma_{av}|$ with enhancing T_{ox} correlates tightly with the increase in $|\text{grad}\sigma|$. And it is indeed so for the region $T_{ox} > 800$ °C that the presently applied 2 h oxidation time results at each T_{ox} in an oxide thickness $d_{ox} > d_{ox}^c$ (i.e., situated on the plateau region in Fig. 8), from where the close tracking in Fig. 3(a) of σ_{av} with $\delta\sigma/\delta d_{ox}$.

We may now try to correlate the trends in the $[P_b]$-T_{ox} profile [Fig. 3(b)] with stress results.[59] When first addressing the T_{ox} range above 800 °C, it is clear that neither σ_i nor σ_{th} accounts for the mapped T_{ox} dependence of $[P_b]$. But instead, the tracking of the $[P_b]$ data with $-\sigma_{av}$ and $-\delta\sigma/\delta d_{ox}$ appears close, apart, perhaps, from some scatter in the data for the $T_{ox} = 800$–900 °C range. That correlation between the latter quantities is highlighted in Fig. 9 where $[P_b]$ data are plotted versus $-\sigma_{av}$ and $-\delta\sigma/\delta d_{ox}$ values read from the fitted curves in Fig. 3(a). The straight lines in Fig. 9 represent least-squares fits, described by

$$[P_b](10^{12}\ \text{cm}^{-2}) = 13.3 - 0.002\,82\delta\sigma/\delta d_{ox}(10^{15}\ \text{dyn/cm}^3) \quad (5)$$

and

$$[P_b](10^{12}\ \text{cm}^{-2}) = 8.27 - 0.987\sigma_{av}(10^9\ \text{dyn/cm}^2)\ , \quad (6)$$

both with a correlation coefficient r of 0.97. Both fits are equally excellent, a finding not totally unexpected in view of the aforementioned close relationship between both stress terms. This reveals the predominant role of σ_{av} in *intrinsic* P_b generation. This correlated decrease of σ_{av} and $[P_b]$ with growing T_{ox} above ≈ 800 °C, and in particularly the finding that $[P_b] \to 0$ for $T_{ox} \to 1150$ °C, fits perfectly with the SiO_2 refractive index data.[60] This index, which is accepted to be a good measure of the oxide density and stress, is seen to decrease monotonically with increasing T_{ox}, to level out at ≈ 1.460 for $T_{ox} > 1150$ °C.

Bjorkman, Fitch, and Lucovsky[53] have concluded from

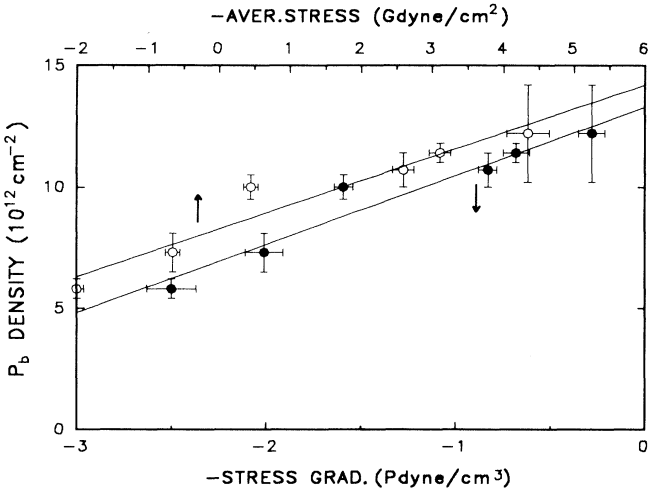

FIG. 9. Correlation of the density of intrinsically generated P_b's at (111)Si/SiO_2 interfaces (observed after degassing) grown in dry O_2 with stress in the SiO_2 layer for the range $T_{ox} = 800$–1100 °C. The solid lines represent least-squares fit [cf. relations (5) and (6)] from where a close linear correlation is noticed.

stress analysis on (100)Si that a correlation[61] exists between the midgap interface state density D_{it} and σ_{av}. As the P_{b0} and P_{b1} defects at the (100) interface account for the major part of the D_{it} states, and if assuming a similar behavior of P_{b0}, P_{b1} and P_b at the (100) and (111)Si/SiO_2 interfaces, respectively, the present findings corroborate the previous D_{it} results, at least for that part correlating D_{it} with σ_{av}. No correlation, however, has been traced by Bjorkman, Fitch, and Lucovsky between D_{it} and the stress gradient, in contrast with the present work. There may be various reasons for this discrepancy, such as the limited number of samples scanned in the stress analysis work. (Noteworthy in this respect is that the stress data as obtained from the straight laser beam defection technique appear somewhat in disconcert with those inferred from ir measurements regarding the evolution of stress with d_{ox}.) Or, perhaps, it could simply bear out a dissimilarity between both interface types.

Within the framework of the mentioned "viscoelastic" relaxation in combination with effects imposed by different thermal history on the various layers in the oxide film, it is expected that the particular stress present in a (111)Si/SiO_2 structure would be the one corresponding to the highest processing temperature it has been submitted to,[62] i.e., either T_{ox} or any other postoxidation anneal temperature T_{an} (evidence for this in terms of D_{it} may also be found in Refs. 53, 61, and 63). Among others, this would tell us that the intrinsic P_b density can be significantly reduced only by treatments at $T > 1000$ °C. It is recalled that here we are dealing with the *intrinsic* elimination of P_b's, not with any kind of chemical complexing of P_b's (for example, HP_b formation) that may passivate the defect, but not eliminate the defect entity.

It is concluded from the $T_{ox} > 800$ °C range that the dominant driving force controlling P_b generation is σ_{av}

intimately related with the near-interfacial stress gradient;[64] $[P_b]$ decreases linearly with $-\sigma_{av}$ and $-\delta\sigma/\delta d_{ox}$, whereby it needs to be recalled that $\delta\sigma/\delta d_{ox}$ is a positive quantity. Of interest for practical work is that the data indicate that intrinsic generation of P_b's is avoided for $T_{ox} \geq 1150\,^{\circ}C$, an unattainable situation for any lower T_{ox}. That absence then of P_b defects appears to be a consequence of the steep drop of interfacial stress in the immediate oxide layers.

We now turn to the $T_{ox} < 800\,^{\circ}C$ range. It is observed that, apart from the $T_{ox} \leq 200\,^{\circ}C$ results, all $[P_b]$ values situate in the range $(9.5-11)\times 10^{12}$ cm^{-2} [see Fig. 3(b)]. From this, in combination with the $T_{ox}=800-1050\,^{\circ}C$ data, it follows that the intrinsic P_b density is effectively pinned within the window $(9.5-12)\times 10^{12}$ cm^{-2} over the range $200 < T_{ox} < 1050\,^{\circ}C$. This must be seen as paramount evidence for the fact that P_b generation in this range is essentially a result of the intrinsic interface stress—there exists little interfacial stress gradient within that T_{ox} range. This is also embedded in Eq. (5), showing that for $\delta\sigma/\delta d_{ox} \rightarrow 0$, the intrinsic P_b density generated is $\approx 13\times 10^{12}$ cm^{-2}, which is to be seen as the amount generated by $\sigma_i = -4.6\times 10^9$ dyn cm^{-2}.

A previous discussion has asserted that the P_b density in a particular Si/SiO_2 structure is set by the highest temperature of thermal cycling it has been submitted to, provided, of course, that this has been continued sufficiently long as to allow the system to reach thermodynamical equilibrium at that temperature through relaxation. It is seen, however, in Fig. 3(b) that the P_b values in the $T_{ox}=450-700\,^{\circ}C$ range (all samples having been submitted to a 1-h vacuum treatment at $\approx 790\,^{\circ}C$ as the final step) are somewhat lower than the value $\approx 11\times 10^{12}$ cm^{-2} found on average for the $T_{ox}=800\,^{\circ}C$ samples. The difference, however, is not large and may have various reasons. A first possibility is insufficient (vacuum) annealing time at 790 °C, i.e., $t_{dh}=1$ h *vis-à-vis* $t_{ox}=2$ h. Second, the small difference could refer to a second-order influence of the ambient type during thermal cycling, that is, the difference between vacuum ($p < 10^{-6}$ Torr) and 1.1 atm O_2.

Also included in Fig. 3(b) are P_b densities measured on as-oxidized (111)Si/SiO_2 entities, showing at least two aspects of interest: One is the observation that $[P_b]$ is fairly constant over the whole oxidation range covered, except for the part $T_{ox} > 1050\,^{\circ}C$, where it declines. The other is that $[P_b]$ increases significantly after exhaustive dehydrogenation, i.e., $[P_b] < [P_b^*]/2$, except, again, for $T_{ox} > 1050\,^{\circ}C$ where the as-oxidized and degassed data tend to merge. The generally much lower P_b density observed on as-oxidized samples is clearly to be ascribed to passivation by H either present as an impurity in the flushed O_2 or diffusing from the ambient through the walls of the silica oven insert. While it appears that the incorporation of H (HP_b formation) occurs equally efficient over the range $T_{ox} < 1050\,^{\circ}C$, the merging of $[P_b]$ and $[P_b^*]$ for as-oxidized samples for $T_{ox} > 1050\,^{\circ}C$ is likely a consequence of less efficient hydrogenation at those high T_{ox}'s, resulting from a changed balance between the passivation [Eq. (1)] and activation [Eq. (2)] reactions, possibly in interplay with[23] trapping of atomic H. For clarity, though, it should be added that *full* P_b passivation does happen for all $T > 220\,^{\circ}C$ when the ambient H concentration is high enough.[9,25]

The evolution of the P_b density over the whole T_{ox} range may thus be synopsized by stating that an almost constant interface stress $\sigma_i = -4.6$ Gdyn/cm^2 accounts for an intrinsic P_b^* density of $\approx (9.5-12)\times 10^{12}$ cm^{-2} of which a fixed part, depending on the actual oxidation setup, is passivated by uncontrolled H incorporation during oxidation.

It is clear from the literature, though, that large variations in the as-oxidized P_b density have been reported for $T_{ox} < 1050\,^{\circ}C$, depending on the employed oxidation device and ambient (see, e.g., Refs. 2–5, 14, and 21). This has been confirmed in the present oxidation setup as we have noticed strong variations in the as-grown P_b density with varying contents of H_2O and H_2 in the oxidizing gas. So the particular P_b density found in an Si/SiO_2 entity is more likely a trademark of the used oxidation facility combined with gas purity, rather than an intrinsic interface feature. In effect, when discussing *intrinsic* interface defect levels, the hydrogen parameter has to be separated. This is believed to have been successfully effectuated along the outlined procedure.

B. Variations in resonance field

Shifts in the ESR resonance field B_0 (read at the zero crossing of the $dP_{\mu a}/dB$ spectrum) may have various origins. Most fundamental is when it concerns a basic atomic aspect of the defect studied, that is, g shifts resulting from changes in the overlap of crucial defect orbitals as a result of slight atomic rearrangements. On the other hand, it may have a more "apparent" spectroscopic origin (e.g., demagnetizing fields, altered average orientation of the defect, etc.), the basic structure (and hence g) of each paramagnetic entity remaining unchanged. Or else, somewhat in between, a g shift may result from altering the interaction strength of the studied spin system with a second spin system of a different g value.

Tracing the correct line shift origin is thus a prime issue. It will be evidenced (*vide infra*) that the shift in the P_b signal (translated into g variations), seen to effectuate in the range $T_{ox}=700-900\,^{\circ}C$ in Fig. 5(b), stems from basic changes in the P_b g matrix. This then leads us to a somewhat deeper analysis of the atomic nature of this effect.

The principal values of the P_b g matrix are generally quoted[5–7,15] as $g_{zz}=g_{\parallel}=2.0014\pm 0.0001$ and $g_{xx}=g_{yy}=g_{\perp}=2.0086\pm 0.0003$. It reflects axial symmetry of the center about the [111] direction perpendicular to the (111)Si/SiO_2 interface, in line with the C_{3v} symmetry of the basic structure of the defect pictured in Fig. 10. Watkins and Corbett, in a pioneering work,[65] provided quantitative understanding using simple molecular-orbital (MO) theory. They showed, among others, that the hole-like g dyadic for such an unpaired bond is axial about the unsaturated bond direction with $g_{\parallel}=g_{fe}$ and $g_{\perp}=g_{fe}+\Delta g_{\perp}$, where

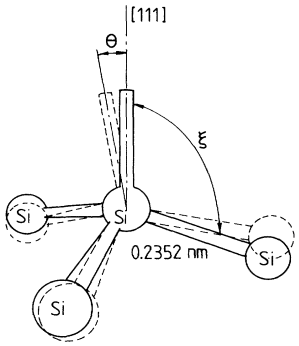

FIG. 10. Basic structure of the P_b defect. The dashed drawing outlines a tilting of the basic Si triangle over an angle Θ relative to the initial configuration, where the bonding angle ξ remains fixed.

$$\Delta g_{\perp} \approx \lambda_{3p}[(1+\gamma)/E_b - (1-\gamma)/E_a]\beta^2 \tag{7}$$

and

$$\gamma = -(\lambda_{2p,3p}\varepsilon_{2p})/(\lambda_{3p}\beta) \approx 0.17 \ . \tag{8}$$

Here, the λ_i represent spin-orbit constants, ε_{2p} an overlap integral, while E_b and E_a represent the energies to the defect bonding and antibonding levels, respectively. The shift $\Delta g_{\perp}$ is seen to be proportional to β^2, the amount of $3p_{[111]}$-like character in the unpaired bond $\alpha|s\rangle + \beta|p\rangle$. While unavoidably oversimplified, this model provided two clear insights: no g shift is to be expected to first order for $\mathbf{B}\|$ unpaired bond direction, while predicting a positive shift in $g_{\perp}$, thus well accounting for the salient features of the P_b g dyadic.

Later, in an attempt to account for the observed $g=2.0055$ value for unpaired bonds[66] in a-Si, quantitative extended Hückel theory (MO) calculations were applied[67,68] to the model cluster shown in Fig. 10, leading to the values $g_{\|}=2.0027$ and $g_{\perp}=2.0076$. This is in fair agreement with the principal P_b g values, which, however, may be rather fortuitous in light of the limited cluster size invoked. But more important for the present analysis is that when allowing for structural modifications of the basic P_b structure, the changes in g are dominated by variations in the angle ξ between the unpaired bond and the adjacent sp^3 bonding hybrids (cf. Fig. 10), rather than the Si-Si bond length: $g_{\|}$ is found to decrease from 2.0027 to 2.0025 by relaxing the defect Si atom inward by 0.33 Å (decrease in ξ of $\sim 8.3°$).

From these simplified calculations then, and assuming linear relationships, it follows that the observed decline of $\sim 0.000\,08$ in g for T_{ox} crossing the 700 °C region [cf. Fig. 5(b)] corresponds to an inward relaxation, on average, of the central Si atom over $\approx (0.000\,08/0.0002)\times 0.33$ Å ~ 0.13 Å, implying a decrease in bonding angle ξ of 3.3°. That relaxation, in terms of g values, is apparently completed for $T_{ox} \gtrsim 950$ °C, where the average P_b defect has thus tended to a more planar, p-like structure. A reasoning then in stress terms would suggest that the P_b defects for the range $T_{ox} \lesssim 700$ °C are, on average, under compressive stress, implying that they would pertain more to the oxide than the Si layer. But this reasoning is probably too naive and should be put in the perspective of the growing evidence that the Si/SiO_2 interface, rather than being perfectly abrupt, extends over about two monolayers of Si—claimed to be fairly insensitive to preparation conditions (see, e.g., Ref. 69). To this needs to be added the possibility of voids[32] and Si inclusions[33,70] in interfacial SiO_2 layers.

Another interpretation may start from the existence of a stress-induced distribution in the unpaired bond direction[40,49] around the "ideal" [111] direction in the $T_{ox} < 700$ °C range. The observed decrease then in g when increasing T_{ox} above ≈ 700 °C is ascribed to the collapse of that distribution as a result of the global relaxation of the SiO_2 layer at high T_{ox} thus releasing interface stress. This model will be elaborated upon when analyzing line shapes (see Sec. IV C).

The defect's inward relaxation may be interpreted in the light of a recent excellent work[71] on P_b using the spin-dependent recombination (SDR) technique in combination with appropriate positioning of the Fermi level in the near-interfacial Si layers of the studied metal-oxide-semiconductor field-effect transistor (MOSFET). Variations were reported in the ^{29}Si P_b hf structure correlated with the energy position of the defect in the band gap. The altering sp^3 hybridization ratios of the unpaired bond, as revealed by the varying hf tensor, were translated into changes in bond angle based on the relation

$$\cos(\xi) = -\alpha^2/(3-\beta^2) \ , \tag{9}$$

derived[72] from simple MO theory. This work demonstrated that the structure of P_b's closer to the valence-band edge is more planar (relaxed) than of those higher up in the gap. The work thus established experimentally that the lower-energy state of P_b is linked to a more planar basic structure, as expected.[12] It is inferred from that work that a "vertical" decrease $\Delta h \approx 0.111$ Å, corresponding to a reduction in $\psi \equiv \xi - 90°$ of 2.8° of the apex Si atom implies a drop of ≈ 0.23 eV in P_b-defect energy[73] E. This $dE/d\psi$ value of ~ 0.082 eV/deg may be compared with the theoretical result of ~ 0.057 eV/deg—almost constant throughout the Si band gap—obtained by a tight-binding approach for a Bethe-lattice terminated cluster.[74] So, we may derive that the above reported enhanced relaxation of the average P_b defect when T_{ox} crosses the 700–900 °C range would correspond to a mean shift over about $(0.13/0.11)\times 0.23$ eV ≈ 0.27 eV of P_b distribution towards the valence band. The density of P_b's in the lower part of the gap has increased at the cost of those in the upper part.

As a final remark, we note that the SDR work[70,71] did not resolve any change in g correlated with the variations in hf interaction. But, in light of the present finding, it is clear that tuning E_F in the Si layers adjacent to the Si/SiO_2 interface should be attendant with g shifts.

C. Linewidth and shape

Linewidth and line-shape data are best analyzed in combination with the g results. The linewidth of the de-

gassed samples remains fixed at 2.6±0.15 G for $T_{ox} < 700\,^{\circ}C$, to descend to a lower plateau of 1.9±0.1 G for $T_{ox} \rightarrow 900\,^{\circ}C$, a general trend much like the g behavior (see Fig. 5). This striking similarity refers to a common mechanism underlying the exposed T_{ox} dependences of g and ΔB_{pp}. In this respect, we note that the characteristic temperature $T_{ox}^{c} \approx 700\,^{\circ}C$, above which both g and ΔB_{pp} start to decrease, coincides well with the threshold T_{ox} value demarcating the onset of the drop in the average stress in the SiO_2 layer as a result of cooperative structural relaxation. Hence, the common underlying factor is likely the impact of local "lattice" relaxation affecting the P_b's.

A third key result in this analysis, almost mirroring the g and ΔB_{pp} vs T_{ox} data, is the variation in line-shape symmetry over the studied T_{ox} range, as exemplified in Fig. 11. That symmetry is essentially a two-case situation: In the lower-T_{ox} range ($\leq T_{ox}^{c}$), the line shape always exhibits a typical asymmetry, that is, $A/B < 1$, with a tendency of A/B to decrease along with T_{ox}; A and B represent the height of the low- and high-field peaks of the $dP_{\mu a}/dB$ spectrum, respectively (see Fig. 11). But upon entering the $T_{ox} > 850\,^{\circ}C$ range, the signal gradually changes to perfect symmetry ($A/B = 1$) and remains so for all higher-T_{ox} values; representative signals observed at 355 ($A/B = 0.87$) and 939 °C ($A/B = 1$) on degassed

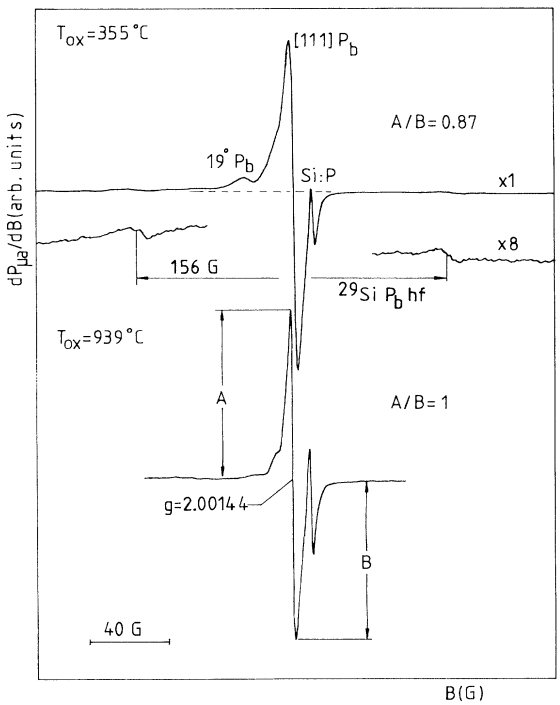

FIG. 11. Representative [111]P_b ESR spectra for the low- ($T_{ox} < 800\,^{\circ}C$) and high- ($T_{ox} > 800\,^{\circ}C$) T_{ox} ranges as observed at 4.3 K for $\mathbf{B} \perp (111)Si/SiO_2$ interfaces grown in dry O_2. Though both signals correspond to $\approx 11 \times 10^{12}$ cm^{-2} P_b's, notice the profound change in line shape (symmetry) upon entering the high-T_{ox} region, with attendant disappearance of the 19° P_b signal ($g = 2.0078$) (see Ref. 15).

(111)Si/SiO_2 structures are displayed in Fig. 11. Again, the T_{ox} value demarcating the transformation of asymmetric into symmetric signals coincides with T_{ox}^{c}, indicating the strong correlation of the P_b line shape with the local structure of the defect. And thus, over the lower-T_{ox} range, it is likely that a significant contribution to ΔB_{pp} (and to the line shape, in general) arises from strain-induced g dyadic broadening,[14,40,75] described by a standard deviation $\sigma_{g_\parallel}$ in $g_\parallel$, on top of the unresolved ^{29}Si hf and DD broadenings.[14,25]

The strain data [cf. Fig. 3(a)] tell us that no measurable relaxation of stress in the SiO_2 occurs in the low-T_{ox} range, well in accord with the fixed values of ΔB_{pp} and g in that range. But when cooperative film relaxation sets in significantly, i.e., $T_{ox} > 900\,^{\circ}C$, both observables tend to their minima. In terms of the ΔB_{pp} data then, this means that the average spread $\sigma_{g_\parallel}$ narrows significantly—an effect that apparently goes hand in hand with a lowering of the mean g (towards $\approx 2.001\,36$), attendant with a shift of the P_b level distribution (D_{it}) towards the valence band. The fact then that ΔB_{pp} levels off [cf. Fig. 3(a)] at $T_{ox} > 900\,^{\circ}C$, while the pertinent SiO_2 film stress keeps shrinking, must mean that the $\sigma_{g_\parallel}$ broadening has become much inferior to the remaining broadening mechanisms, in agreement with previous detailed analysis:[14,40] The latter indeed concluded that $\sigma_{g_\parallel} \rightarrow 0$, that is, insignificant strain broadening in (111)Si/SiO_2 entities grown at 900–925 °C for $\mathbf{B} \| [111]$. We should emphasize, though, that the latter conclusion does not apply to any other direction of $\mathbf{B}$, as an average standard deviation $\sigma_{g_\perp} = 0.000\,75$–$0.000\,93$ in $g_\perp$ has been deduced.[14,40,75]

It thus follows in the low-T_{ox} range there to exist a non-negligible spread in $g_\parallel$, in agreement with previous work on the (111)Si/native oxide structure.[47,75] But before proceeding, we should make clear that variations in DD-induced broadening ΔB_{pp}^{DD}, being proportional to f in the diluted range (i.e., $f < 0.003$, where f is the fractional occupancy of lattice sites by P_b defects), cannot account for the drop in ΔB_{pp} when entering the high-T_{ox} range. Although the change is small, the P_b density is seen to increase rather than decrease in that T_{ox} range, so that, if anything, ΔB_{pp} should have increased. The dipolar contribution to the P_b signal width has been analyzed in detail[25] for $\mathbf{B} \perp (111)Si/SiO_2$ interface comprising an intrinsic density $[P_b] \approx 1.2 \times 10^{13}$ cm^{-2}. There it was found that the DD interaction added a width $\Delta B_{pp}^{DD} = 0.61 \pm 0.05$ G on top of the residual natural width (that is, width devoid of DD broadening) $\Delta B_{pp}^{R} = 1.29 \pm 0.03$ G.

The origin of the spread in $g_\parallel$ has been addressed before. Within the context of P_b defects, such spread could mainly arise from two effects: First, it could be ascribed[40,49] to a distribution of the unpaired bond directions around the "ideal" [111] direction [perpendicular to the (111)Si/SiO_2 interface] resulting from enhanced strain—a distribution in the angle Θ between the unpaired bond direction and [111] [a highly restricted version of the common "powder effect" in ESR studies (see, e.g., Ref. 44)]. It is envisioned in a first approximation as

resulting from a strain-induced tilting of the basic P_b-defect pyramid (cf. Fig. 10) over an angle Θ, different from P_b site to site, but into first order leaving the g tensor unchanged: In other words, an identical g tensor is slightly tilted differently from site to site. Along this model, the collapse in $\sigma_{g_\parallel}$ effectuating in the high-T_{ox} range indicates that thermal annealing of film stress leads to local relaxation of the P_b's so as to better align their unpaired bond direction with [111].

In the second case, the spread in $g_\parallel$ might be due to slight relative atomic (Si) displacements that lead to statistical variations in wave-function overlap. The simplest way to picture this is perhaps variations in the vertical position (cf. Fig. 10) of the central Si atom resulting from the lateral stress exerted on the backbonded basic Si triangle. While these displacements may not ensue shifts in $g_\parallel$ into first order,[65] they do so in second order as pointed out by detailed MO calculations.[67]

ESR signal simulations will be carried out for $\mathbf{B}\|[111]$ within the framework of both models as to extract basic information regarding the physical mechanism underlying the observed systematic variation in B_0. This is best accomplished by combined analysis of all three crucial observations, i.e., dependence on T_{ox} of ΔB_{pp}, g, and line shape. Hence, signal simulation is subject to three strict criteria that must be met simultaneously when upwards crossing T_{ox}^c: (1) narrowing of ΔB_{pp} from 2.6 to 1.9 G, (2) a decrease of $\delta g \approx 0.0001$ in g (from 2.001 44 to 2.001 36), (3) perfect symmetrization of the line shape (A/B changing from ~ 0.8 to 1).

In the unpaired bond *direction distribution model,* a Gaussian distribution in Θ characterized by the standard deviation σ_Θ and centered at $\Theta=0$ ([111] direction; $g=2.001\,36$) will be assumed, given as

$$h(\Theta)=\frac{1}{\sqrt{2\pi}\sigma_\Theta}\exp[-\tfrac{1}{2}(\Theta/\sigma_\Theta)^2] \ . \tag{10}$$

When inserting into line-shape simulations, it is clear from powder spectra analysis that this $h(\Theta)$ has to be multiplied by $\sin\Theta$ (the solid angle effect; see, e.g., Ref. 44 and references therein) to incorporate the statistical probability for finding a P_b unpaired bond tilted over a particular angle Θ. $h(\Theta)$ is easily put into magnetic field units using

$$\Theta=\arcsin\left[\frac{(h\nu/\mu_B B)^2-g_\parallel^2}{g_\perp^2-g_\parallel^2}\right]^{1/2} , \tag{11}$$

as derived from the relation

$$B=h\nu/\mu_B g \ , \tag{12}$$

where $g^2=(g_\parallel\cos\Theta)^2+(g_\perp\sin\Theta)^2$ for axial symmetry. In Eq. (11), ν is the microwave frequency and μ_B is the Bohr magneton. The distributions $h(\Theta)$ and $h(\Theta)\sin(\Theta)$ are depicted in Fig. 12(a) both in field and Θ units. It is clear that this model will lead to an average decrease of B_0 (apparent increase of g).

The second model, starting from a distribution in $g_\parallel$, requires deeper consideration as it is evident that numerous kinds of distributions may be forwarded, depending on the particular range one deems appropriate for $g_\parallel$ variation. One plausible guideline, though, seems the above outlined "vertical displacement of the central Si atom" analysis (see Sec. IV B) indicating that no $g_\parallel$ *lower* than the $g_\parallel^r$ value characterizing the fully relaxed P_b structure is to be expected. So, we should first of all select the correct $g_\parallel^r$ value. And again, within the context of the forwarded stress analysis, it is plausible that this pertains to the T_{ox} range where stress has largely relaxed, that is, $T_{ox}>950\,^\circ$C, so that $g_\parallel^r \equiv 2.001\,36$. The fact that $g_\parallel$ does not keep shrinking (as well as correlated contributions to ΔB_{pp} and signal distortion) when further enhancing T_{ox} just means that the strain broadening in $g_\parallel$ has become negligible already at $T_{ox}\approx 950\,^\circ$C. The value of $g_\perp$ is fixed at 2.0087, the correct value being somewhat immaterial for the present $\mathbf{B}\|[111]$ case. This leads us to approximate the distribution $k(g_\parallel)$ in $g_\parallel$ by a *hemi-Gaussian* "centered" at $g_\parallel=g_\parallel^r$, as pictured in Fig. 12(b), both in field and g units. Other models might suppose *symmetric* Gaussian distributions in $g_\parallel$, centered at $g_\parallel^r$ or any other (close) $g_\parallel$ value. These, however, have to be discarded at once as they can never lead to asymmetric

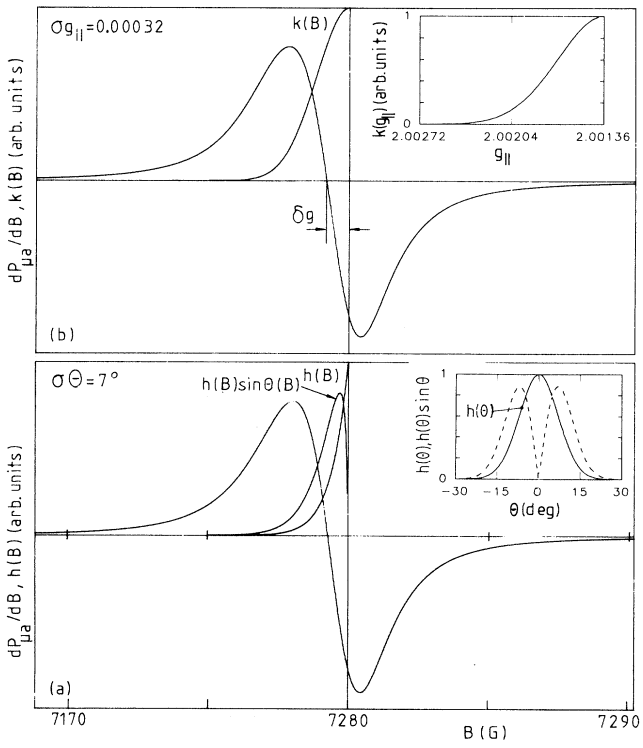

FIG. 12. Computer-calculated absorption-derivative P_b ESR spectra (20.390 GHz) for $\mathbf{B}\perp(111)\mathrm{Si/SiO_2}$ interfaces grown in the low-T_{ox} range ($<800\,^\circ$C). (a) and (b) represent the models incorporating a Gaussian unpaired bond direction distribution and a Gaussian spread in $g_\parallel$, respectively, leading to the pictured $h(B)$ and $k(B)$ distributions. A Lorentzian of $\Delta B_{pp}^L=1.9$ G was used as the convoluting line in both cases. The parameters were optimized to fit the experimental width $\Delta B_{pp}=2.6$ G. A shift $\delta g \equiv g-2.001\,36$ of 0.000 24 and 0.000 21 is obtained for the Θ and $g_\parallel$ spread models, respectively.

line shapes (as observed in the low-T_{ox} range) and, moreover, seem to conflict with the reasonable assumption that there exists one type of preferential stress at the interface, i.e., either compressive or tensile.

The next step in the signal simulation then requires the (constituent) line shape (and width) the proposed g spread profiles need to be convoluted with to obtain the ultimate P_b signal shape. This constituent shape may be derived from deeper perusal of the observed line shapes and broadening mechanisms. As alluded to, when the signal narrows from 2.6 to 1.9 G on traversing the $T_{ox} \approx 700\,^{\circ}\mathrm{C}$ region, this narrowing is ascribed to the disappearance of the strain broadening in g, the latter thus accounting for ≈ 0.7 G broadening. An in depth analysis of the P_b signal for $\mathbf{B}\perp(111)\mathrm{Si/SiO_2}$ structure grown at $\approx 930\,^{\circ}\mathrm{C}$ has shown the high-T_{ox} 1.9-G peak-to-peak width to comprise a significant contribution of 0.6 G due to DD interaction (Lorentzian-like shape[25]), the remaining natural signal of $\Delta B_{pp}^{R} = 1.29 \pm 0.03$ G exhibiting a Voigt-like structure composed of a constituent Lorentzian and Gaussian broadening function with peak-to-peak widths of 0.67 and 0.90 G, respectively.[25] The overall dominance of the Lorentzian part leads us to approximate the high-T_{ox} 1.9-G signal by a Lorentz curve[76] (in fair agreement with experiment[14]). This is then further employed as the constituent convoluting signal.

And as the $g_{\parallel}$ spread distribution is assumed Gaussian, it is expected that the 2.6-G signal is largely[77] Voigt-like. Using then the accurate formula

$$\Delta B_{pp}^{T} = \tfrac{1}{2}\Delta B_{pp}^{L} + [(\Delta B_{pp}^{G})^2 + \tfrac{1}{4}(\Delta B_{pp}^{L})^2]^{1/2} , \qquad (13)$$

where ΔB_{pp}^{T}, ΔB_{pp}^{L}, and ΔB_{pp}^{G} represent the total, Lorentzian, and Gaussian linewidths of the Voigt shape, allows us to estimate the contribution ΔB_{pp}^{G} originating from the g spread in the low-T_{ox} range. Inserting the values $\Delta B_{pp}^{L} = 1.9$ G and $\Delta B_{pp}^{T} = 2.6$ G renders $\Delta B_{pp}^{G} = 1.35$ G.

Subsequently, optimized (that is, meeting the constraint $\Delta B_{pp} = 2.60$ G) absorption-derivative spectra have been computed for the $T_{ox} < 700\,^{\circ}\mathrm{C}$ range. Figures 12(a) and 12(b) show the results, corresponding to $\sigma_{g\parallel} = 0.000\,32$ and $\sigma_{\Theta} = 7^{\circ}$ for the $g_{\parallel}$ and Θ spread models, respectively; the corresponding apparent shift $\delta g = g - g_{\parallel}^{r}$ away from the measured high-T_{ox} value is given by 0.000 21 and 0.000 24, while the asymmetry parameter $A/B = 0.86$ and 0.8 for the $\sigma_{g\parallel}$ and σ_{Θ} models, respectively. The fit for the $g_{\parallel}$ distribution model (dotted line) to the resonance observed on a $\mathrm{Si/SiO_2}$ sample grown at $T_{ox} = 651\,^{\circ}\mathrm{C}$ is also displayed in Fig. 13, from where an excellent fit of the asymmetry and the central part of the spectrum is noticed [the nonfitting wing structure is as expected, as the (partly) resolved structure in the experimental signal results from two-dimensional dipolar[25] and superhyperfine[12,14,25,78] interaction, which has not been included in the simulation]. But it is clear from Fig. 12 that the computed curves for both models show little difference, and indeed, the fitting quality for both models is found to be almost equal. The $\sigma_{g\parallel}$ model, though, is more favored because it leads to a smaller apparent g shift (i.e., 0.000 21) and slightly larger A/B,

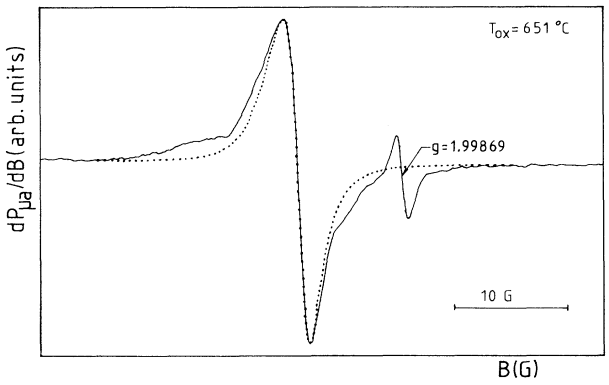

FIG. 13. Fit of the $g_{\parallel}$-spread model calculation [dotted curve; see also Fig. 12(b)] to the P_b signal measured at 4.3 K for $\mathbf{B}\perp(111)\mathrm{Si/SiO_2}$ interface grown at 651 °C. The dotted curve was calculated for $\sigma_{g\parallel} = 0.000\,32$, using a Lorentzian of $\Delta B_{pp}^{L} = 1.9$ G as the convoluting signal.

more in accord with experiment—a conclusion in line with the above interpretation of the g shift (based on the average relaxation of the P_b entity towards a more planar structure) seen to occur on crossing the $T_{ox} \approx 700\,^{\circ}\mathrm{C}$ region. The truth, however, is probably in between as both effects may be operative, the $\sigma_{g\parallel}$ effect being somewhat more pronounced. If one admits, in an idealized way, that the $g_{\parallel}$ and Θ spreads are, respectively, associated with vertical and lateral displacements of the defect Si atom relative to the bulk, this result then seems in line with previous Rutherford backscattering studies,[79] concluding that the first two Si monolayers next to the interface exhibit a larger vertical (≈ 0.2 Å) than lateral (0.1 Å) displacement.

The above discrimination between the two models considered has largely been based on two experimental ESR quantities, namely, the resonance zero crossing (apparent g shift) and line-shape asymmetry. For clarity then, we add that, while DD effects are clearly revealed in the line shape and width, the DD interaction has no impact on the signal's average resonance frequency (g factor) nor signal symmetry, the basic physical reason being that it concerns an *internal* interaction within a one-species spin system—unable to alter the system's average parameters.[80] Moreover, the variation in P_b density, and hence DD interaction, over the transition region $T_{ox} = 700$–$800\,^{\circ}\mathrm{C}$ is insignificant, anyhow.

It is realized that the fit obtained with $g_{\parallel}$ spread model is still not perfect, but is considered close in light of the approximations made and can certainly be improved when dealing with a more complex line-shape structure. Anyhow, the line-shape fitting data do seem to exclude the predominance of unpaired bond tilting (σ_{Θ} model) in causing P_b line-shape asymmetries in the range $T_{ox} = 200$–$800\,^{\circ}\mathrm{C}$. Note, however, that the latter effect may well dominate in the as-grown (111)Si/native oxide structure, where a "large" shift in $g_{\parallel}$ [cf. Fig. 5(b)] is observed.

It is interesting to analyze the deduced $g_{\parallel}$ spread in terms of atomic displacements. Along the g factor calculations presented in Ref. 67, the above result

$\sigma_{g\parallel}=0.000\,32$ obtained for $T_{ox}<700\,^{\circ}C$ would correspond to a rms variation of ~ 0.53 Å in the vertical position of the defect Si atom. (This value may be somewhat exaggerated due to theoretical oversimplification in Ref. 67, but it nevertheless indicates the trend.) This may be compared with the high-T_{ox} value: in his work on strain broadening of the P_b resonance, Brower derives from the excess line broadening of the P_b ^{29}Si hf signals that a small rms spread of ~ 0.02 Å in vertical displacement is left[14,81] after oxidation at $\approx 900\,^{\circ}C$. This then leads us to the following global picture regarding structural relaxation of the P_b defect: Upon increasing T_{ox} above $\sim 700-800\,^{\circ}C$, the rms variation in the vertical position of the defect Si atom of ≈ 0.53 Å, existing in the low-T_{ox} range, narrows drastically to ≈ 0.02 Å, attendant with an average inward relaxation of the defect Si atoms from its tetrahedral position toward the bulk of ~ 0.13 Å. This cogently exposes the profound differences in the nature of the low- and high-T_{ox} Si/SiO_2 interfaces.

In summary, it follows that the P_b line-shape and g phenomena are well accounted for by (weak) vertical displacements of the apex Si atom with respect to the (111)Si/SiO_2 interface in the low-T_{ox} range. These displacements largely disappear in the high-T_{ox} range, the P_b defects now tending to their fully relaxed state, characterized by $g_{\parallel}=2.001\,36$ and $\Delta B_{pp}=1.9$ G for $[P_b]=1.2\times 10^{13}$ cm^{-2}.

Somewhat disconcerting is the T_{ox} dependence of ΔB_{pp} for $T_{ox}>1050\,^{\circ}C$ [Fig. 5(a)] as one would expect ΔB_{pp} to decline from 1.9 G to ~ 1.30 G as a result of the drop in $[P_b]$ [cf. Fig. 3(b)] with a corresponding vanishing of the DD broadening. While ΔB_{pp} does not exhibit such decline, the ΔB vs T_{ox} plot, in contrast, does. This ΔB_{pp} behavior is presently not understood.

Within the context of the DD interaction, the line-shape factor results shown in Fig. 7 are well in line with the $[P_b]$ vs T_{ox} data. It has previously been outlined[25] that, when there is a significant DD interaction within a *two-dimensional* spin system, κ may reach "unrealistically" high values, that is, exceeding those of the singular, well-known line shapes, namely, Gaussian, Lorentzian, and Voigt profile (κ given as 1.03, 3.63, and $1.03\leq\kappa\leq 3.63$, respectively). With the adopted definition of the line-shape factor, it points to a multicomponent signal reflecting the dipolar structure. This DD structure is (partially) resolved here, in contrast with the well-known three-dimensional case, as a result of the insufficient averaging (i.e., number of spins in the shells surrounding a particular spin) of the DD interaction over the third dimension.

In broad terms, it may thus be stated for the dehydrogenated samples that κ is large ($\sim 5-7$) over the range $T_{ox}\leq 960\,^{\circ}C$. And although there appears to be some dip in the $T_{ox}=500-700\,^{\circ}C$ range, the constantly high κ values are well in line with the $[P_b]$ vs T_{ox} plot [compare Figs. 3(b) and 7]. Apart from the 22 °C point, all spin density data situate in the range $(9.5-14)\times 10^{12}$ cm^{-2}, the high value of which accounts for the DD line-shape distortion, indeed. But in the high-T_{ox} ($>960\,^{\circ}C$) range, κ is seen to decrease monotonically, almost mirroring the drop in $[P_b]$, down to the value 3.5 ± 0.25 for $T_{ox}=1140\,^{\circ}C$. And the expectation is that, for $T_{ox}>1150\,^{\circ}$, it will level off at the value 2.0, previously deduced for the residual signal:[25] It is expected that the shape of this signal will be dominated by unresolved ^{29}Si hf structure due to interaction with neighboring ^{29}Si nuclei.[14,25] It is obvious that the latter structure will depend little on T_{ox} as the chemical structure of P_b remains unaffected.

V. CONCLUSIONS

A comparative analysis has been presented of the characteristics of the K-band P_b ESR signal observed at 4.3 K on dry (111)Si/SiO_2 structures, obtained after 2 h oxidation, for the oxidation range $22-1140\,^{\circ}C$. While it received little attention in the past, such a comparative study is generally hampered by the (partially) passivating effect of uncontrolled amounts of hydrogen inevitably introduced during oxidation. This makes the separation of the H impact prerequisite, which has been realized in this work by appropriate postoxidation degassing in vacuum for about 1 h at 790 °C. This treatment is believed to essentially leave all intrinsically generated P_b entities, i.e., P_b^*, unpassivated (thus ESR active)—or at least putting all Si/SiO_2 structures on an equal comparative footing regarding incorporated H. And as it has been argued that $[P_b^*]$ is set by the highest temperature of thermal cycling (provided that thermal equilibration is allowed), the $T_{ox}\geq 790\,^{\circ}C$ range is expected to be the most informative. This has allowed a reliable comparison of the salient P_b ESR properties with relevant stress data for the Si/SiO_2 entity. After exhaustive dehydrogenation, this has led to the following main results.

(1) $[P_b^*]$ is found to be confined to the narrow range $(9.5-14)\times 10^{12}$ cm^{-2} for all $T_{ox}\leq 1050\,^{\circ}C$, except[48] at $T_{ox}=22\,^{\circ}C$, where a value of $\sim 2\times 10^{13}$ cm^{-2} is observed. Beyond this T_{ox} range, $[P_b^*]$ drops monotonically, tending to below 10^{10} cm^{-2} (i.e., the detection limit) for $T_{ox}\rightarrow 1150\,^{\circ}C$. The P_b densities of as-oxidized samples are generally less than half of those observed after dehydrogenation (due to initial partial H passivation) for the range $T_{ox}\leq 1050\,^{\circ}C$, above which both densities merge.

(2) A linear relationship is found between $[P_b^*]$ and σ_{av}, the average compressive stress in the Si-oxide film. Generation of P_b's is thus seen to vanish in the range $T_{ox}>1050\,^{\circ}C$ in perfect correlation with the full (cooperative) rearrangement of the interface region. That T_{ox} range for restructuring of the oxide is in reassuring agreement with the range previously deduced from changes in refractive index.[82]

(3) $g_{\parallel}$ remains fixed at $2.001\,44\pm 0.000\,03$ for all $T_{ox}<700\,^{\circ}C$, whereupon it declines toward $g_{\parallel}=2.001\,36\pm 0.000\,03$ for $T_{ox}\rightarrow 950\,^{\circ}C$. Comparison with theoretical work indicates that this decline is the signature of relaxation of the P_b's towards a slightly more planar structure. An average displacement of the defect central Si atom towards the back Si triangle over ~ 0.13 Å has been deduced, attendant with a downward shift of

the P_b level (D_{it}) distribution in the Si band gap over about 0.27 eV. The effect is attributed to the disappearance of the strain distribution in $g_{\parallel}$, characterized by $\sigma_{g_{\parallel}}=0.000\,32$, as a result of oxide restructuring.

(4) The peak-to-peak linewidth closely mirrors that $g_{\parallel}$ pattern; ΔB_{pp} is observed to decline from 2.6 ± 0.15 G for $T_{ox}\lesssim 700\,^{\circ}\mathrm{C}$ towards 1.9 ± 0.1 for $T_{ox}\rightarrow 950\,^{\circ}\mathrm{C}$.

(5) The behavior of the line-shape factor confirms the previous findings. A large κ, in the range 5.1–7.5, is observed for $T_{ox}\lesssim 1000\,^{\circ}\mathrm{C}$, reflecting the profound impact of (partially resolved) dipolar fine structure on the line shape, in agreement with theoretical analysis for such a diluted two-dimensional P_b spin system of $[P_b]\approx 12\times 10^{12}\ \mathrm{cm}^{-2}$. Above that range, κ drops steadily, tending to the value 3.5 ± 0.25.

(6) An isotropic ESR signal, termed the *EX* center and characterized by $g=2.002\,46\pm0.000\,03$ and $\Delta B_{pp}=1.0\pm0.1$ G, is observed in the as-grown Si-oxide films in the range $T_{ox}=700$–$850\,^{\circ}\mathrm{C}$. It is ascribed to an *intrinsic* defect, not primarily related with impurities in the Si oxide. What is important is that it is observed in *as-grown* thermal oxide, in contrast with the common ESR-active defects that are only observed after damaging the Si-oxide by irradiation with some kind of energetic particles.

Within the framework of ESR observability, the present experiments have delimited the conditions for growing (111)Si/SiO_2 structures intrinsically "free" of P_b defects. A required condition is oxidation at temperatures in excess of $\sim 1150\,^{\circ}\mathrm{C}$ as to allow the full (cooperative) restructuring of the a-SiO_2 film. In that T_{ox} range there apparently exists a stress-free match between the c-Si substrate and the superficial thermal a-SiO_2 layer.

The unveiled strong correlation between $[P_b]$ and σ_{av} indicates that for the *pure* Si/SiO_2 system, there seems no way, below $T_{ox}\sim 1140\,^{\circ}\mathrm{C}$, to grow a (111)$Si/SiO_2$ interface intrinsically free of P_b defects, whatever the growth conditions or initial Si surface geometry: The obstructing strain is naturally set. It thus appears that in order to realize a P_b-defect free Si/SiO_2 interface in the $T_{ox}<1150\,^{\circ}\mathrm{C}$ range, it must imply the incorporation of other chemical substances.

[1]Y. Nishioka, Eronides F. da Silva, Jr., and T. P. Ma, Appl. Phys. Lett. **52**, 720 (1988); W. L. Warren and P. M. Lenahan, IEEE Trans. Nucl. Sci. **NS-34**, 1355 (1987).

[2]For a recent review on Si-SiO_2 defect physics, see the 13 papers in Semicond. Sci. Technol. **4**, 961 (1989), and references therein.

[3]Y. Nishi, J. Appl. Phys. **10**, 52 (1971).

[4]P. J. Caplan, E. H. Poindexter, B. E. Deal, and R. R. Razouk, J. Appl. Phys. **50**, 5847 (1979).

[5]E. H. Poindexter, P. J. Caplan, B. E. Deal, and R. R. Razouk, J. Appl. Phys. **52**, 879 (1981).

[6]K. L. Brower, Appl. Phys. Lett. **43**, 1111 (1983).

[7]E. H. Poindexter and P. J. Caplan, Prog. Surf. Sci. **14**, 211 (1983).

[8]R. E. Mikawa and P. M. Lenahan, Appl. Phys. Lett. **46**, 550 (1985); K. L. Brower, P. M. Lenahan, and P. V. Dressendorfer, *ibid.* **41**, 251 (1982).

[9]K. L. Brower, Appl. Phys. Lett. **53**, 508 (1988); Phys. Rev. B **38**, 9657 (1988).

[10]A. Stesmans and K. Vanheusden, Phys. Rev. B **44**, 11 353 (1991).

[11]K. L. Brower, Z. Phys. Chem. **151**, 177 (1987).

[12]A. H. Edwards, Phys. Rev. B **36**, 9638 (1987).

[13]J. H. Stathis and L. Dori, Appl. Phys. Lett. **58**, 1641 (1991).

[14]K. L. Brower, Phys. Rev. B **33**, 4471 (1986).

[15]A. Stesmans, Appl. Phys. Lett. **48**, 972 (1986); Z. Phys. Chem. **151**, 191 (1987).

[16]E. H. Poindexter, G. J. Gerardi, M.-E. Rueckel, P. J. Caplan, N. M. Johnson, and D. K. Biegelsen, J. Appl. Phys. **56**, 2844 (1984).

[17]S. T. Chang, J. K. Wu, and S. A. Lyon, Appl. Phys. Lett. **48**, 662 (1986).

[18]G. J. Gerardi, E. H. Poindexter, P. J. Caplan, and N. M. Johnson, Appl. Phys. Lett. **49**, 348 (1986).

[19]N. M. Johnson, D. K. Biegelsen, M. D. Moyer, S. T. Chang, E. H. Poindexter, and P. J. Caplan, Appl. Phys. Lett. **43**, 563 (1983); N. M. Johnson, Wei Shan, and P. Y. Yu, Phys. Rev. B **39**, 3431 (1989).

[20]H. G. Grimmeiss, W. R. Buchwald, E. H. Poindexter, P. J. Caplan, M. Harmatz, G. J. Gerardi, D. J. Keeble, and N. M. Johnson, Phys. Rev. B **39**, 5175 (1989).

[21]E. Kooi, Philips Res. Rep. **21**, 477 (1966); T. W. Hickmott, J. Appl. Phys. **48**, 723 (1977); N. M. Johnson, D. K. Biegelsen, and M. D. Moyer, J. Vac. Sci. Technol. **19**, 390 (1981).

[22]D. M. Brown and P. V. Gray, J. Electrochem. Soc. **115**, 761 (1968).

[23]K. L. Brower and S. M. Myers, Appl. Phys. Lett. **57**, 162 (1990).

[24]D. L. Griscom, J. Appl. Phys. **58**, 2524 (1985).

[25]A. Stesmans and G. Van Gorp, Phys. Rev. B **42**, 3765 (1990); **45**, 4344 (1992).

[26]D. L. Griscom, J. Electron. Mater. **21**, 763 (1992).

[27]B. E. Deal and A. S. Grove, J. Appl. Phys. **36**, 3770 (1965).

[28]M. A. Hopper, R. A. Clarke, and L. Young, J. Electrochem. Soc. **122**, 1216 (1975).

[29]N. F. Mott, S. Rigo, F. Rochet, and A. M. Stoneham, Philos. Mag. B **60**, 189 (1989).

[30]E. A. Irene, CRC Crit. Rev. Solid State Mater. Sci. **14**, 175 (1988).

[31]S. Aptekar, M. Fernandes, and D. L. Kwong, J. Electrochem. Soc. **132**, 1449 (1985).

[32]Bent Nielsen, K. G. Lynn, D. O. Welch, T. C. Leung, and G. W. Rubloff, Phys. Rev. B **40**, 1434 (1989); E. A. Irene, J. Electrochem. Soc. **125**, 1708 (1978).

[33]J. Halbritter, J. Mater. Res. **3**, 506 (1988).

[34]W. Kern and D. A. Poutinen, RCA Rev. **31**, 187 (1970).

[35]A. Stesmans and J. Braet, Surf. Sci. **172**, 389 (1986).

[36]See, e.g., M. Grundner and H. Jacob, Appl. Phys. A **39**, 73 (1986).

[37]A. Stesmans and G. Van Gorp, Rev. Sci. Instrum. **60**, 2949 (1989).

[38]"Exhaustive" in this context does not imply that there may be no H left in the Si/SiO_2 system. What is meant, instead, is that further anneal in vacuum does not result in ESR activation of any additional P_b entities by the release of H.

[39]K. L. Brower, Phys. Rev. B **42**, 3444 (1990).

[40]A. Stesmans and J. Braet, in *Insulating Films on Semiconductors,* edited by J. J. Simonne and J. Buxo (North-Holland, Amsterdam, 1986), p. 25.

[41]A similar, though weak and H-uncontrolled, trend is discerni-

ble in Refs. 5 and 70.

[42]Brower, in contrast, has reported that postoxidation anneal in vacuum for 1 h at 850 °C left the P_b signal unchanged. The lack of observation of any P_b signal enhancement could be due to two reasons: First, there is the possibility that the oxidation setup did not suffer from any H pollution. So, all P_b entities intrinsically generated during oxidation at 750 °C end up ESR active as no H-passivation effect could have occurred. This explanation, however, conflicts with the quoted P_b density of $\approx 3\times 10^{12}$ cm^{-2}, which is about 4 times less than the intrinsic number presently derived. Second, a totally opposite possibility is that Brower's thermal treatment setup suffers from a hidden constant source of H, so that the post-oxidation dehydrogenation anneal remains without any effect.

[43]A. Stesmans, Phys. Rev. B **45**, 9501 (1992).

[44]For a recent review on E' defects, see, e.g., D. L. Griscom, Glass Sci. Technol. B **4**, 151 (1990).

[45]R. L. Beadles, in *Handbook of Material Sciences III,* edited by C. T. Lynch (CRC Press, Cleveland, OH, 1975), p. 123.

[46]C. A. Swenson, J. Phys. Chem. Ref. Data **12**, 179 (1983).

[47]A. Stesmans, Appl. Surf. Sci. **30**, 134 (1987).

[48]Note that the native oxides studied are likely to constitute more of a chemical than a thermal oxide, as these oxides were "grown" at RT in air ambient on Si wafers that received RCA precleaning. Indeed, the final step of the latter cleaning involves treatment in the $HCl:H_2O_2:H_2O$ mixture which, in fact, constitutes an acid-catalyzed oxidation resulting in a chemical oxide layer (mainly SiO_2) of ≈ 1 nm (see Ref. 36).

[49]A. Stesmans, J. Braet, J. Witters, and R. F. Dekeersmaecker, Surf. Sci. **141**, 255 (1984).

[50]E. Kobeda and E. A. Irene, J. Vac. Sci. Technol. B **4**, 720 (1986).

[51]E. Kobeda and E. A. Irene, J. Vac. Sci. Technol. B **6**, 574 (1988).

[52]J. T. Fitch, C. H. Bjorkman, G. Lucovsky, F. H. Pollak, and X. Yin, J. Vac. Sci. Technol. B **7**, 775 (1989).

[53]C. H. Bjorkman, J. T. Fitch, and G. Lucovsky, Appl. Phys. Lett. **56**, 1983 (1990).

[54]M. Jarosz, L. Kocsanyi, and J. Giber, Appl. Surf. Sci. **14**, 122 (1982).

[55]R. J. Jaccodine and W. A. Schlegel, J. Appl. Phys. **37**, 2429 (1966).

[56]E. P. Eernisse, Appl. Phys. Lett. **30**, 290 (1977).

[57]"Viscous flow" is likely a misconception in this context, a more correct term being structural relaxation; see A. G. Revesz, B. J. Mrstik, and H. L. Hughes, in *Proceedings of a Symposion on the Physics and Technology of Amorphous SiO_2,* edited by R. A. B. Devine (Plenum, New York, 1987), p. 297; R. W. Rendell and K. L. Ngai, Appl. Phys. Lett. **57**, 2428 (1990); and Ref. 82.

[58]There remains, however, some discussion of whether the observed ν_{ir} vs d_{ox} profile should be interpreted as resulting from a gradual change in SiO_2 stoichiometry rather than a decrease in stress, when moving away from the interface.

[59]Our P_b data probably pertain to the slow cooling rate (cf. Ref. 54). As depicted in Fig. 2, sample cooling is closely exponential, the fastest rate of ≈ 8 °C/s occurring initially (cf. Fig. 2).

[60]See, e.g., B. Leroy, Philos. Mag. B **55**, 159 (1987).

[61]The conclusion that D_{it} may essentially be reduced to zero by high-T annealing has been reached before by A. G. Reesz, K. H. Zaininger, and R. J. Evans, J. Phys. Chem. Solids **28**, 197 (1967). This behavior was attributed to a structural rearrangement of the Si/SiO_2 phase boundary, and, in addition, these authors also unveiled a clear correlation between D_{it} and the final oxidation rate, the Si surface orientation, and H_2 treatments.

[62]Particularly strong evidence for this comes from SiO_2 refractive index measurements. See, e.g., L. M. Landsberger and W. A. Tiller, Appl. Phys. Lett. **51**, 1418 (1987); and Ref. 82.

[63]E. Kobeda and E. A. Irene, J. Vac. Sci. Technol. B **5**, 15 (1987).

[64]The correlation with the near-interfacial stress gradient is perhaps not unexpected. The larger the gradient, that is, the faster with depth into the SiO_2 film the stress can fully relax, the smaller the total transverse force mutually exerted by both substances, so the lower the P_b density generated.

[65]G. D. Watkins and J. W. Corbett, Phys. Rev. **134**, A1359 (1964).

[66]M. H. Brodsky and R. S. Title, Phys. Rev. **23**, 581 (1969).

[67]N. Ishii, M. Kumeda, and T. Shimizu, Jpn. J. Appl. Phys. **20**, L673 (1981); **20**, L920E (1981).

[68]Note that, while the calculations in Ref. 67 were generally carried out on 13-atom model clusters, the cluster considered for the simple unpaired Si bond was restricted to the basic four-atom Si cluster shown in Fig. 10.

[69]F. J. Himpsel, F. R. McFeely, A. Taleb-Ibrahimi, J. A. Yarmoff, and G. Hollinger, Phys. Rev. B **38**, 6084 (1988).

[70]Y. Ohji, Y. Nishioka, K. Yokogawa, K. Mukai, Q. Qiu, E. Arai, and T. Sugano, IEEE Trans. Electron. Devices **37**, 1635 (1990).

[71]M. A. Jupina and P. M. Lenahan, IEEE Trans. Nucl. Sci. **37**, 1650 (1990).

[72]C. A. Coulson, *Valence* (Oxford University Press, London, 1961), p. 203.

[73]Strictly speaking, through analysis of $(111)Si/SiO_2$ structures, the P_b sp hybridization vs energy has been probed only for the lower half of the Si band gap; the data in Ref. 71 for the upper half of the gap were obtained on $(100)Si/SiO_2$, where P_{b0} and P_{b1} constitute the pertinent interface defects. So, unless these behave identically to the P_b centers—an item under much debate (cf. Refs. 12 and 13)—extrapolation of the P_b behavior based on P_{b0} and P_{b1} data is not permitted. Hence the value $dE/d\psi \sim 0.08$ eV/deg, obtained for P_b in the lower half of the gap, is used throughout the whole band gap, which is well in line with theory (Ref. 74).

[74]P. A. Fedders and A. E. Carlsson, Phys. Rev. B **39**, 1134 (1989).

[75]A. Stesmans, Semicond. Sci. Technol. **4**, 1000 (1989).

[76]Note that this can be only a first-order approximation as it has been demonstrated that the P_b signal corresponding to $[P_b]\approx 10^{13}$ cm^{-2} is distorted by partly and unresolved dipolar fine structure; it nevertheless appears to be a fair approximation (see Ref. 14).

[77]In practice, the measured signal is asymmetric ($A/B < 1$), so that the shape cannot be strictly Voigt-like.

[78]M. Cook and C. T. White, Phys. Rev. Lett. **59**, 1741 (1987); Phys. Rev. B **38**, 9674 (1988).

[79]R. Haight and L. C. Feldman, J. Appl. Phys. **53**, 4884 (1982).

[80]J. H. Van Vleck, Phys. Rev. **74**, 1168 (1948).

[81]From $\sigma_{g\perp}$, however, Brower found an rms spread of ≈ 0.2 Å in vertical displacement of the defect Si atom (see Ref. 14). But he cautiously added that this value should be considered as an extreme upper limit, as various effects have not been taken into account in deriving that conclusion. The result from P_b ^{29}Si hf data is considered more reliable.

[82]K. Taniguchi, M. Tanaka, and C. Hamaguchi, J. Appl. Phys. **67**, 2195 (1990).